Space Science Reviews (2023) 219:36
https://doi.org/10.1007/s11214-023-00981-z

Small-Scale Dynamos: From Idealized Models to Solar and Stellar Applications

Matthias Rempel[1] · Tanayveer Bhatia[2] · Luis Bellot Rubio[3] · Maarit J. Korpi-Lagg[2,4,5]

Received: 17 March 2023 / Accepted: 7 June 2023 / Published online: 4 July 2023

Abstract
In this article we review small-scale dynamo processes that are responsible for magnetic field generation on scales comparable to and smaller than the energy carrying scales of turbulence. We provide a review of critical observation of quiet Sun magnetism, which have provided strong support for the operation of a small-scale dynamo in the solar photosphere and convection zone. After a review of basic concepts we focus on numerical studies of kinematic growth and non-linear saturation in idealized setups, with special emphasis on the role of the magnetic Prandtl number for dynamo onset and saturation. Moving towards astrophysical applications we review convective dynamo setups that focus on the deep convection zone and the photospheres of solar-like stars. We review the critical ingredients for stellar convection setups and discuss their application to the Sun and solar-like stars including comparison against available observations.

Keywords Small-scale dynamo · Stellar magnetism · Quiet Sun · Cool stars · Convection

1 Introduction

The Sun is the only star that can be scrutinized in detail at high spatial and temporal resolution. Observations show that magnetic fields are ubiquitous in the quiet Sun—the areas of the solar surface away from active regions and the enhanced network. They cover the whole solar surface, all the time, irrespective of the phase of the solar cycle. Quiet Sun (QS) fields can be classified into network and internetwork (IN) fields. The former are relatively strong and vertical, and occupy the outer boundaries of supergranular cells. The latter are weaker and highly inclined, and can be found in the cell interiors. In high-resolution observations, both fields are detected as magnetic flux concentrations of opposite signs organized on subarcsecond scales. Observations of quiet Sun magnetism over the past few decades have lent growing support for a dynamo process that operates in the IN independently from the large-scale dynamo (LSD) responsible for the solar cycle. We provide a detailed review of solar observations in Sect. 2.

The theoretical concept of a small-scale dynamo (SSD) instability, independent of the presence of symmetry-breaking effects, such as helicity, dates back to Kazantsev (1968).

Solar and Stellar Dynamos: A New Era
Edited by Manfred Schüssler, Robert H. Cameron, Paul Charbonneau, Mausumi Dikpati, Hideyuki Hotta and Leonid Kitchatinov

Extended author information available on the last page of the article

As identified early on, the magnetic Prandtl number, $\mathrm{Pm} = \nu/\eta$, where ν is the kinematic viscosity and η the magnetic resistivity, plays a critical role for SSD action and we provide a more detailed account of the theoretical concepts in Sect. 3. It was first suggested by Petrovay and Szakaly (1993) that this dynamo instability may be the origin of the weak IN fields.

Numerical simulations of SSD started with convective setups and solar surface simulations with 3D radiative transfer at Pm around one, and have recently been extended towards the numerically more challenging lower Pm-regime. The evolution of numerical models is described in Sect. 4. We focus on investigations of the role of Pm during kinematic and saturated phases (Sect. 4.1), deep convection setups (Sect. 4.2), surface convection setups (Sect. 4.3) and the possibility of an SSD in the radiative interior of solar-like stars (Sect. 4.4). Section 5 provides an overview of recent applications to solar-like stars. Here we focus on the effects of small-scale magnetism on stellar structure, the basal chromospheric flux and contributions to short-term stellar variability that has to be considered for exoplanet detection. We conclude the review with an outlook in Sect. 6.

2 Solar Observations

Because of their abundance, quiet Sun fields are important contributors to the flux budget of the solar photosphere. The total unsigned longitudinal magnetic flux of the quiet Sun has been estimated to be 8×10^{23} Mx at any time (Gošić 2015), similar to the total flux carried by active regions at solar maximum ($\sim 6 \times 10^{23}$ Mx; Jin et al. 2011). Network fields contribute about 80–85% of this flux, while the IN supplies the remaining 20–15% (Wang et al. 1995; Gošić 2015). However, the IN is extremely dynamic and evolves very rapidly, with flux appearance rates from 120 to 1100 Mx cm^{-2} day^{-1} (e.g., Gošić et al. 2016; Smitha et al. 2017) that surpass those of active regions by orders of magnitude (0.1 Mx cm^{-2} day^{-1}; Schrijver and Harvey 1994). IN fields are also the main contributors to the total energy budget of the solar photosphere (Trujillo Bueno et al. 2004; Rempel 2014).

Pushed and dragged by granular and supergranular convective flows, quiet Sun magnetic fields undergo frequent interactions between them and with other pre-existing fields, particularly in the IN. Such interactions are believed to trigger magnetic reconnection events at different heights in the atmosphere, releasing energy and contributing to the heating of the chromosphere and corona locally and globally. This role has been recognized only recently, as high resolution observations became available both from ground and from space. Quiet Sun fields also contribute to atmospheric heating by channeling waves from the photosphere to higher atmospheric layers (Jess et al. 2023).

To understand these fields we must determine their properties and origin. From an observational point of view, they turn out to be very different from active region fields. For example, IN fields are weaker, more dynamic, and do not show significant changes with the solar cycle (Hinode Review Team et al. 2019). Therefore, it is likely that their origin is also different from the LSD-related active regions and magnetic fluctuations originating from this component through tangling by turbulence. Cascading from large to small scales by active region decay seems not to be viable because of the low flux emergence rate of active regions and the lack of solar cycle variations. An SSD was proposed by Petrovay and Szakaly (1993) as the origin of the weak IN fields. SSD simulations are indeed able to reproduce many statistical properties of IN fields, but important questions remain open, as for example whether or not they can explain the spatial distribution of the flux, the field strength and field inclination distributions, or the flux emergence processes observed in the IN. On the other hand, the quiet Sun network seems to show some variation with the solar cycle

(Korpi-Lagg et al. 2022). The variation is certainly smaller than that of active regions, but it suggests that the network gets contributions from both the LSD and the SSD.

By characterizing the properties, dynamics and temporal evolution of quiet Sun fields observationally, it should be possible to constrain SSD models and help set the most appropriate physical ingredients such as boundary conditions and Pm regimes. For example, a good determination of the magnetic field strength at the surface can provide information on the dynamics of the upper convection zone (CZ), where the bottom boundary condition is usually placed (see Sect. 4.3.1). Also, a detailed characterization of the flux emergence process in granules and intergranular lanes based on high-resolution observations can help validate the mechanisms suggested by numerical simulations. Finally, by studying the formation and evolution of the quiet network, one may get information about the possible interplay and feedback between SSD and LSD.

2.1 Diagnostic Techniques

Our current understanding of quiet Sun fields has been gained through the interpretation of polarimetric measurements of spectral lines formed in the solar photosphere. When the polarization signals are very weak (near the noise level), quantitative analyses are usually not possible and only general properties of the observed signals can be derived, such as their amplitudes, line asymmetries, lifetimes or spatial distribution. However, when the signals are strong it is possible to interpret them by inverting the radiative transfer equation, which gives precise inferences of the vector magnetic field and other atmospheric parameters (see reviews by del Toro Iniesta and Ruiz Cobo 2016; Trujillo Bueno and del Pino Alemán 2022).

The physical mechanisms that leave imprints of the magnetic field on the polarization profiles of spectral lines are the Zeeman and Hanle effects. Both can be used to diagnose the photospheric field, depending on the strength and position of the magnetic features on the solar disk (for details see Bellot Rubio and Orozco Suárez 2019). Zeeman measurements provide spatially resolved observations, but are affected by possible cancellation of the mixed-polarity fields that may coexist in the resolution element. Hanle measurements do not suffer from these cancellation effects, but in turn they are spatially unresolved.

The main problem faced by spectropolarimetric observations of the quiet Sun is that the signals are extremely weak (of order 10^{-3} of the continuum intensity or smaller). To properly detect them, long integrations are needed. This worsens the effective spatial resolution and the cadence of the observations, but also lowers the noise level, which is important to cope with the different sensitivity of the linear and circular polarization signals to weak magnetic fields in the Zeeman regime. Because of such a sensitivity difference, the same amount of noise in linear and circular polarization results in much larger transverse fields than longitudinal fields if interpreted as a real signal. This intrinsic bias is known to affect the determination of the magnetic field components, particularly the field inclination, which is usually inferred to be more horizontal than the true one (e.g., Borrero and Kobel 2011). Indeed, noise is often the main reason for the discrepancies between analyses, hence the need to reduce it as much as possible in the first place and then minimize its effects with appropriate techniques.

In what follows we summarize the main results derived from the observations. Aspects that are particularly relevant for comparison with numerical models include the spatial distribution of the fields on small scales, the mean longitudinal flux density, the magnetic field strength and inclination distributions, their stratification with height, the temporal evolution of the fields (in particular the flux emergence modes), solar cycle variations (total unsigned flux, polarity imbalance, latitudinal distribution), and the impact of quiet Sun fields on the chromosphere.

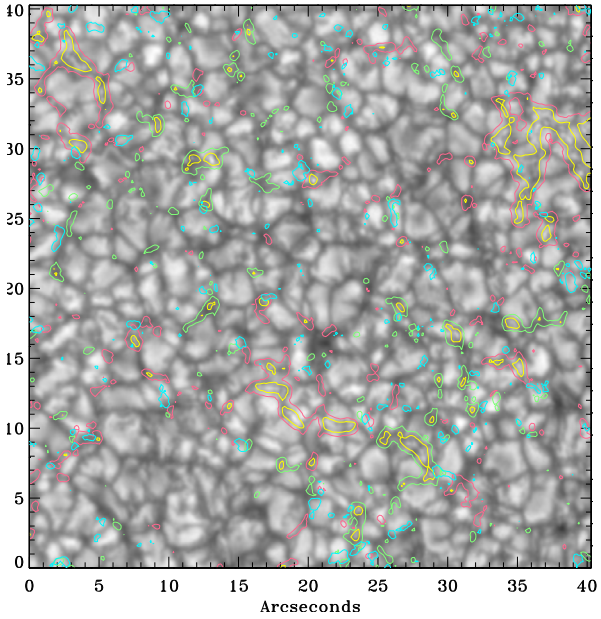

Fig. 1 Spatial distribution of quiet Sun magnetic fields as observed by the Hinode spectropolarimeter (SP) at disk center. Red and green contours show positive and negative apparent longitudinal flux densities larger than 24 Mx cm^{-2} (10 times above the noise level), while the yellow contours show strong longitudinal flux densities of more than 100 Mx cm^{-2}. Blue contours represent apparent horizontal flux densities in excess of 122 Mx cm^{-2} (three times the corresponding noise level). The longitudinal signals are preferentially located in intergranular lanes. The strong horizontal signals are spatially separated from the vertical signals, and are mostly seen above or at the edges of granules. Reproduced with permission from Lites et al. (2008), copyright by AAS

2.2 Properties of Quiet Sun Magnetic Fields

2.2.1 Spatial Distribution on Small Scales

For a long time, quiet Sun magnetic fields were thought to occupy only the intergranular space. However, with sufficient spatial resolution and polarimetric sensitivity, granules also show clear polarization signals. The spatial distribution of the field can be seen in Fig. 1. The fields in intergranular lanes tend to be stronger, more vertical, and more concentrated than in granular cells, which explains their higher visibility. They carry most of the magnetic flux (Beck and Rezaei 2009). However, flux emergence is observed to take place preferentially in granules in the form of small-scale magnetic loops (Centeno et al. 2007; Martínez González and Bellot Rubio 2009; Fischer et al. 2020) and sheets (Orozco Suárez et al. 2008; Fischer et al. 2019), putting constraints on the mechanisms that bring the field to the surface (see Sect. 4.3.1 for details). Once at the surface, the field is dragged by the horizontal granular motions to the intergranular lanes, where it can be further amplified.

2.2.2 Level of Quiet Sun Magnetism

Traditionally, the magnetization of the quiet Sun has been quantified in terms of the longitudinal flux density. This parameter is defined as $\phi = f\, B_{\rm LOS}$, with f the fraction of the

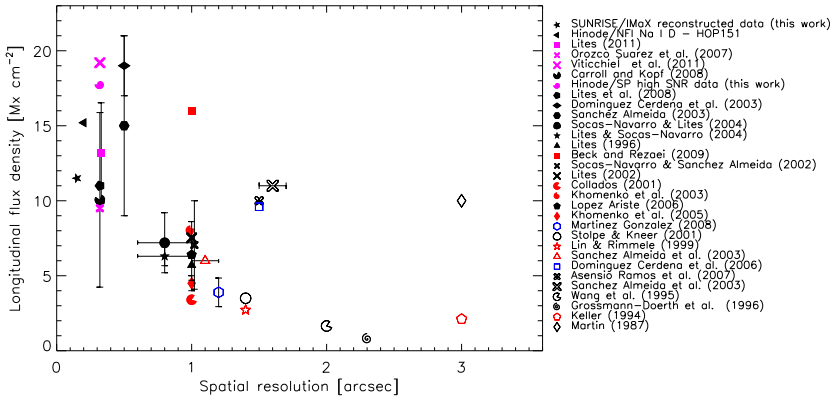

Fig. 2 Compilation of unsigned longitudinal flux densities in the quiet Sun, as a function of the spatial resolution of the observations. From Bellot Rubio and Orozco Suárez (2019)

resolution element covered by the magnetic field (assumed to be homogeneous) and $B_{\rm LOS}$ the longitudinal component of the field. The longitudinal flux density can be derived relatively easily from measurements of the circular polarization profile at a single wavelength or through the inversion of full Stokes profiles, which explains its popularity. In the weak field regime, ϕ is proportional to the circular polarization signal.

Unfortunately, this parameter is very dependent on the spatial resolution and polarimetric sensitivity of the observations. At low spatial resolution, the magnetic filling factor f tends to be small, decreasing the flux density values. Also, the amount of Zeeman cancellation may be significant, especially for magnetograph observations that are not based on full spectral line profiles. This leads to a further reduction of ϕ. The polarimetric sensitivity, on the other hand, affects the estimates through the noise: the larger the noise is, the higher the mean flux density values will be, unless provision is made to exclude pixels without clear polarization signal from the analysis. Therefore, high spatial resolution and high sensitivity are essential for reliable estimations of the flux density in the quiet Sun.

With increasing spatial resolution, the mean unsigned longitudinal flux density derived from Zeeman-sensitive spectral lines increases until approximately 0.5 arcsec, where it levels off and seems to remain constant at about 10–20 Mx cm^{-2} (Fig. 2). The apparent longitudinal flux densities of 7–11 Mx cm^{-2} reported by Danilovic et al. (2010b) from Hinode/SP measurements using the method of Lites et al. (2008) are consistent with these values.

However, despite the apparent agreement between the estimates reported at high spatial resolution, it is important to remember that the longitudinal flux density only provides a lower limit to the intrinsic longitudinal field, as it also depends on the actual filling factor of the observations, which is unknown but certainly different from 1. This dependency makes it very difficult to compare the observed flux densities with simulations, where the magnetic filling factor is always unity. The magnetic field strength is less problematic and should be preferred for quantitative analyses, especially now that powerful techniques are available to retrieve it from the observations.

2.2.3 Field Strength Distribution

Stokes inversions of varying degrees of sophistication have been used to determine the magnetic field strength, field inclination and magnetic filling factor on a pixel by pixel basis

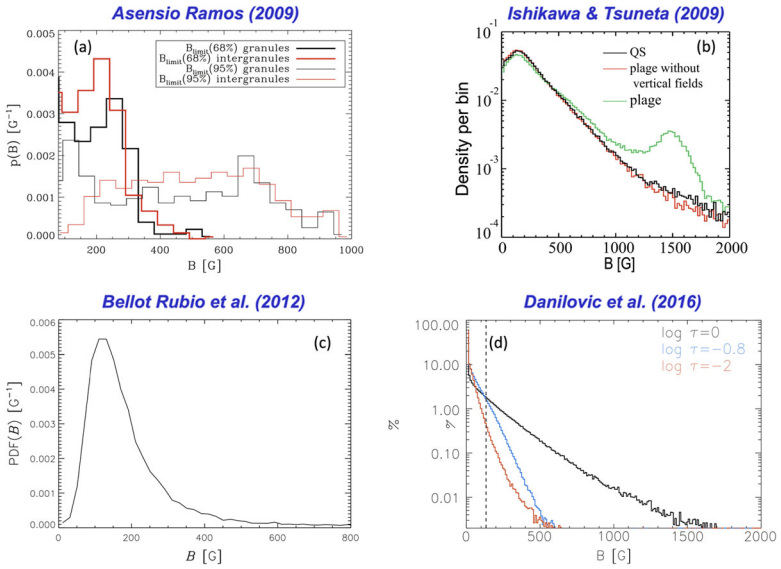

Fig. 3 Field strength distributions in the IN determined from four different inversions of Hinode/SP measurements. Clockwise from top left: Asensio Ramos (2009), Ishikawa and Tsuneta (2009), Bellot Rubio and Orozco Suárez (2012), and Danilovic et al. (2016b). Reproduced with permission, copyright by AAS (panels a, c) and by ESO (panels b, d)

from spectropolarimetric observations of Zeeman sensitive lines. Stokes inversions allow to disentangle the actual contribution of each of these parameters to the longitudinal magnetic flux, providing much richer information. Thus, they are more appropriate for comparison with simulations.

According to the inversions, IN fields are weak for the most part (Fig. 3). Although the details vary between analyses, this conclusion seems to be robust. The field strength distribution shows a preponderance of weak fields in the hG range and a long tail toward kG fields. Network fields tend to be stronger than IN fields, with a hump at 1–1.5 kG. For a summary of these results, see Sect. 4.5 of Bellot Rubio and Orozco Suárez (2019).

From the inferred field strength distribution it is possible to compute the mean field strength over the observed field of view. The resulting values are influenced by the noise of the Stokes profiles, the diagnostic technique employed, and even the way the averaging is done (in particular whether pixels with noisy signals are included or excluded from the analysis). Also the inclusion or exclusion of the network influences the results. But they tend to be much larger than the average longitudinal flux densities shown in Fig. 2. Lites et al. (2008) reported a value of $\langle B \rangle = 185$ G, while Orozco Suárez and Bellot Rubio (2012) found $\langle B \rangle = 220$ G with $\langle |B_z| \rangle = 64$ G, and Danilovic et al. (2016b) derived $\langle B \rangle = 130$ G at $\tau = 1$ with $\langle |B_z| \rangle = 84$ G. These values represent upper limits to the true mean field strengths, as in the first two cases only pixels with clear signals were considered (hence biasing the mean toward the stronger fields) and in the last case all pixels were included (hence adding some contribution from photon noise in pixels with no polarization signal). In general, the field strength is found to decrease with height in the photosphere (Danilovic et al. 2016b). Hanle-effect inversions of molecular lines also show a rapid drop of the field strength with height, from 95 G at $z = 200$ km to 5 G at 400 km (Milić and Faurobert 2012).

These results are compatible with the average field strengths determined from spatially unresolved scattering polarization measurements of the Sr I 460.7 nm line using the Hanle effect. The observed center-to-limb variation of the fractional linear polarization of the Sr I line can be reproduced by a volume-filling magnetic field with an isotropic distribution of orientations and a homogeneous strength of 60 G or, alternatively, an exponential distribution of field strengths with $\langle B \rangle = 130$ G between 200 and 400 km above $\tau = 1$ (Trujillo Bueno et al. 2004). It was concluded that most of the fields contributing to the Hanle depolarization of this line are located in intergranular space and have strengths between 2 and 300 G, well within the Hanle saturation regime. Fields above granules are much weaker and do not seem to contribute significantly to the observed depolarization. By including this small contribution in the fit to the center-to-limb variation of the Sr I linear polarization, an exponential distribution with $\langle B \rangle = 15$ G was inferred in granular cells.

Recent results from multi-line inversions of intensity profiles aimed to avoid the problems of noise in the Stokes polarization spectra also confirm that granules harbor weaker fields (Trelles Arjona et al. 2021). According to these inversions, the average field strength in granules and intergranular lanes is 16 G and 76 G, respectively, in the optical depth range from 1 to 0.1. The average field strength across the field of view is 46 G.

2.2.4 Field Inclination Distribution

The existence of inclined fields in the quiet Sun has been known since the mid 1990s, when small patches of Horizontal Internetwork Fields were discovered and characterized using full Stokes spectropolarimetric measurements at a resolution of about 1 arcsec (Lites et al. 1996). Subsequent analyses at similar resolutions but based on different spectral lines and inversion codes have confirmed them (e.g., Khomenko et al. 2003; Martínez González et al. 2007; Beck and Rezaei 2009).

With the significantly better spatial resolution of 0.3 arcsec provided by the Hinode spectropolarimeter, the transverse apparent flux density in quiet Sun areas at the disk center was found to be about 5 times larger than the longitudinal apparent flux density, suggesting that most of the IN fields are actually very inclined (Lites et al. 2008). Similar results were obtained also from ground-based observations (Beck and Rezaei 2009).

Nearly all the inversions performed to date, using different model atmospheres, codes and assumptions, result in a field inclination distribution at the disk center dominated by highly inclined fields (e.g., Orozco Suárez et al. 2007; Lites et al. 2008; Beck and Rezaei 2009; Orozco Suárez and Bellot Rubio 2012; Asensio Ramos and Martínez González 2014; Danilovic et al. 2016b; Martínez González et al. 2016). Some examples are given in Fig. 4. The distribution usually shows a maximum at 90°, representing horizontal fields, and has tails decreasing toward 0° and 180° (vertical fields). While some contamination by noise cannot be completely ruled out (Borrero and Kobel 2011), it is unlikely that all the inclined fields inferred in the solar IN are a consequence of noise in the linear polarization measurements. Still, the exact shape of the inclination distribution remains a matter of debate, particularly the amplitude of the peak at 90°, which exhibits significant differences between analyses.

Also, there is an ongoing discussion on whether the inclination distribution is isotropic, quasi-isotropic, dominantly horizontal, or dominantly vertical (Bellot Rubio and Orozco Suárez 2019). This is an important question that can shed light on the origin of the fields or the way they appear on the solar surface. Observations outside of the disk center may hold the key to answering it. If the field is isotropic, the inclination distribution should not change with the heliocentric angle. Unfortunately, studies of the center-to-limb behavior of

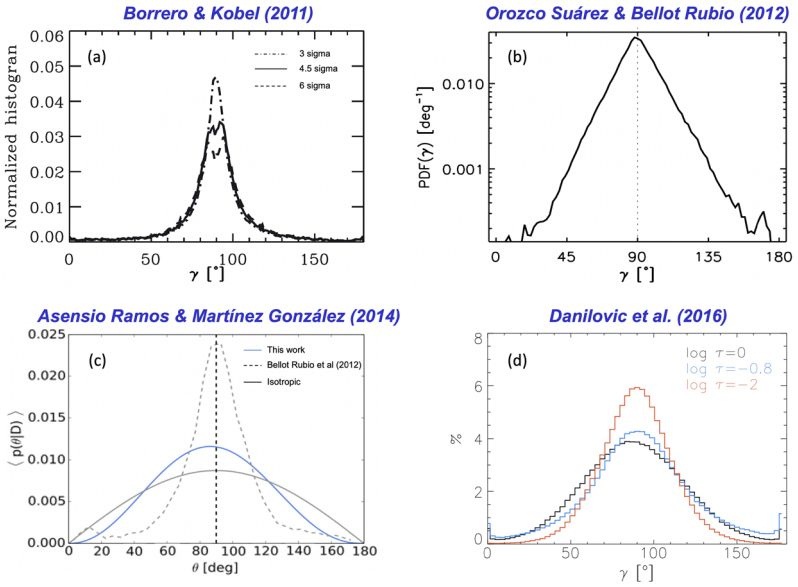

Fig. 4 Field inclination distribution in the solar IN determined from four different inversions of Hinode/SP measurements at disk center. Inclinations are measured with respect to the local vertical, with 90° corresponding to horizontal fields and 0°/180° representing fields pointing to/away from the observer. Clockwise from top left: Borrero and Kobel (2011), Orozco Suárez and Bellot Rubio (2012), Asensio Ramos and Martínez González (2014), and Danilovic et al. (2016b). Reproduced with permission, copyright by ESO (panels a, c, d) and by AAS (panel b)

the inclination distribution are very scarce (e.g., Orozco Suárez and Katsukawa 2012). The efforts have rather focused on determining the variation of the circular and linear polarization amplitudes, since they are not biased by photon noise. The results of these analyses are still controversial, but there seems to be a variation of the weakest polarization signals with heliocentric angle which would not be compatible with an isotropic distribution of field orientations (Lites et al. 2008; Borrero and Kobel 2013; Lites et al. 2014, 2017).

On the simulation side, the field turns out to be predominantly horizontal in the mid and upper photosphere, where most spectral lines used for diagnostics are formed (Sect. 4.3.3). Interestingly, this seems to be a natural outcome of both near-surface magnetoconvection and SSD action. The MHD simulations of Steiner et al. (2008) show a prevalence of inclined fields at a height of 500 km, where the ratio of horizontal to vertical field components is 2 to 5.6, in agreement with Lites et al. (2008). In these simulations, the horizontal field strength reaches a maximum in the upper photosphere because overshooting convective motions expel the horizontal field upwards to layers where vertical flows are no longer present, allowing the field to accumulate there. The same dynamic effect is observed in SSD simulations, resulting in fields that are more horizontal in the upper photosphere and ratios of horizontal to vertical field consistent with the observations (see Schüssler and Vögler 2008; Rempel 2014, and Sect. 4.3.3).

Thus, observed inclination distributions that are predominantly horizontal in the mid photosphere would be compatible with SSD action, but do not necessarily imply its existence. On the contrary, isotropic or quasi-isotropic distributions would pose a serious problem for simulations. Determining which distribution better represents the quiet Sun IN requires higher sensitivity measurements, such as those to be provided by the Daniel K. Inouye Solar

Telescope (DKIST; Rimmele et al. 2020) and the European Solar Telescope (EST; Quintero Noda et al. 2022). The new observations will also allow the height dependence of the field to be examined through inversions with vertical gradients of the parameters. The studies carried out so far suggest that the field inclination varies with height, becoming more horizontal in the mid photosphere (Danilovic et al. 2016b, see Fig. 4d). This may just reflect the existence of small-scale loop-like structures straddling a few granules all over the solar surface, as the loop tops naturally have more horizontal fields and are located higher in the atmosphere than the footpoints, but such an idea requires further observational verification.

2.3 Flux Emergence in the Quiet Sun

Magnetic flux emergence is an ubiquitous process in the quiet Sun. It happens on a wide range of spatial scales (from mesogranular to granular and subgranular scales) and on short timescales, but long duration observations are needed to characterize its statistical properties. Such observations are difficult to obtain, as they require stable conditions for hours. IN magnetic fields appear on the solar surface in two flavors: as bipolar pairs or clusters of mixed-polarity elements, and as individual unipolar features. The latter are features of given polarity without any clear associated opposite-polarity element in the surroundings (Fig. 5a). It has recently been shown that about 55% of the total IN flux appears in bipolar form, while the rest is unipolar (Gošić et al. 2022). The physical properties of these two populations turn out to be different, which suggests different origins.

Studying the modes of appearance of quiet Sun fields before they interact with photospheric convective flows is key to understanding their nature through comparisons with numerical simulations. Small-scale bipolar emergence occurs in the form of magnetic Ω-loops (Centeno et al. 2007; Martínez González and Bellot Rubio 2009) and magnetic sheets (Fischer et al. 2019). Magnetic loops emerge into the photosphere above or at the edges of granules, showing linear polarization in between two-opposite circular polarization patches (Fig. 5b). These signals represent the horizontal field of the loop top and the vertical field of the loop legs, respectively. The linear polarization signals show up prominently in high-sensitivity spectropolarimetric observations (Danilovic et al. 2010a; Ishikawa and Tsuneta 2010, 2011; Martínez González et al. 2012; Kianfar et al. 2018; Gošić et al. 2021). It has been suggested that the magnetic topology of these loops may explain the field strength and field inclination distributions observed in the quiet Sun IN (Lites et al. 2008; Bellot Rubio and Orozco Suárez 2019). Small-scale loops are common features in magnetoconvection simulations (e.g., Stein and Nordlund 2006; Abbett 2007; Moreno-Insertis et al. 2018) and SSD simulations (Schüssler and Vögler 2008; Danilovic et al. 2010b), where they are seen as individual entities or as bundles thereof.

Horizontal magnetic fields flanked by vertical fields have been observed to emerge also in granular lanes produced by horizontal vortex tubes (Fischer et al. 2020). An example is shown in Fig. 5c. The magnetic field has a loop-like structure with strengths of several hundred G and is detected at the late stage of the granular lane development, similarly to the loops described above. However, the formation mechanism seems to be different. The vortex tube grabs pre-existing horizontal fields in the adjacent intergranular lanes, located at or below the surface, and takes them to the granular interior, where they are transported to the surface and eventually back to the intergranular space by the granular upflows. In this way, vortex tubes provide a mechanism for the local recirculation of magnetic field required by the SSD to operate on the solar surface (Sect. 4.3.1).

Another type of bipolar flux emergence in the quiet Sun involves large sheets of horizontal fields covering a full granule (Fischer et al. 2019, see Fig. 5d), which has been identified

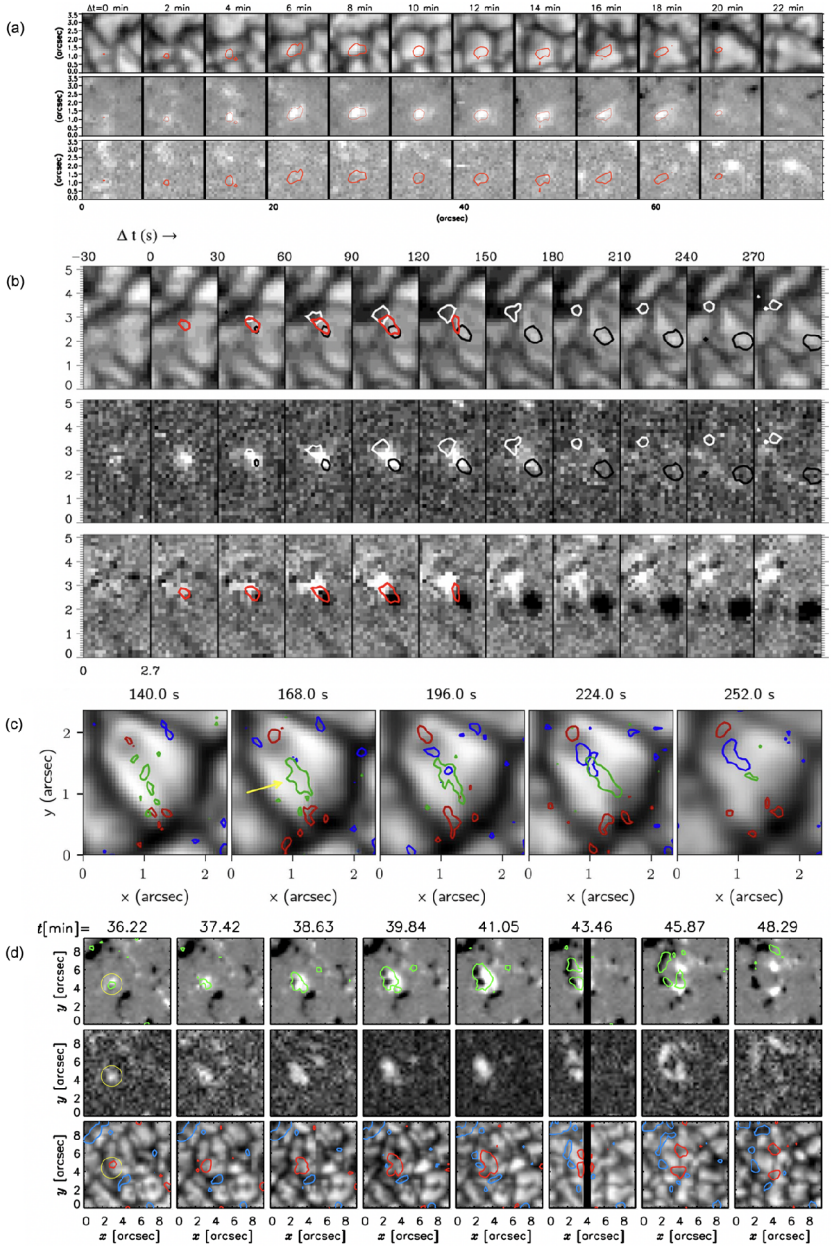

Fig. 5 Examples of magnetic flux appearance in the quiet Sun. (a) Unipolar features. (b) Bipolar magnetic loops. (c) Horizontal fields in granular lanes. (d) Sheets of horizontal fields covering a granule. The different rows show continuum intensity, circular and linear polarization in (a), continuum intensity, linear and circular polarization in (b), continuum intensity in (c), and circular, linear polarization and continuum intensity in (d). Circular polarization patches are indicated with red contours in (a), white and black contours in (b), and red and blue contours in (c) and (d). Linear polarization patches are outlined with red contours in (b) and green contours in (c) and (d). Adapted from Orozco Suárez et al. (2008), Martínez González and Bellot Rubio (2009), Fischer et al. (2020), and Fischer et al. (2019). Reproduced with permission, copyright by ESO (panels a, d) and by AAS (panels b, c)

also in simulations (Moreno-Insertis et al. 2018). The sheet fragments as it expands to the granular edges, leaving only the footpoints that can be observed as opposite-polarity patches in circular polarization maps. This form of flux emergence may explain the small clusters of mixed-polarity elements observed in longitudinal magnetograms such as those analyzed by Gošić et al. (2022), but an unambiguous confirmation is not possible until the appearance sites of the cluster members are determined.

While bipolar flux emergence should be considered the dominant form of flux appearance in the quiet Sun, unipolar appearances still provide a considerable fraction of the magnetic flux present on the solar surface. However, they pose an important problem, as the opposite polarity that must be associated with every unipolar feature seems to be missing. Clearly, this is a detection problem. Very likely, the signals are there but cannot be seen due to insufficient polarimetric sensitivity. Indeed, it has been suggested that these unipolar features do not bring new magnetic fields to the solar surface, but are the result of very weak background flux that is hidden in the noise until some mechanism concentrates it, becoming visible above the detection threshold (Lamb et al. 2008; Gošić et al. 2022). The exact mechanism is presently unknown, but it might be related to converging horizontal flows at mesogranular lanes and vertices (Yelles Chaouche et al. 2011; Requerey et al. 2017). Also the nature of the background flux is unknown, in particular whether it would be produced by SSD action or by the LSD.

Upon appearance on the solar surface, magnetic fields interact with the local granular motions and are dragged by supergranular flows towards the edges of the supergranular cells (e.g., Gošić et al. 2014). Bipolar features can be followed for some time until the footpoints cancel or merge with other magnetic features, losing their identity. Both the magnetic topology and the evolution of these features carry information on the origin of the fields, and are therefore important parameters to be compared with numerical simulations. A specific open question is the role of IN fields in the formation of the quiet network outlining the boundaries of supergranular cells. This will be briefly discussed in the following section.

2.4 Contribution of the IN to the Quiet Sun Network

The quiet Sun network is believed to be formed by active region decay, ephemeral regions and IN fields. It shows a variation with the solar cycle, which reflects its connection with the LSD (see Sect. 2.5). However, the contribution of the various components to the network flux is still under discussion.

It has been shown using Hinode/SOT data that about 40% of the total IN flux eventually ends up in the quiet Sun network (Gošić et al. 2014). According to those observations, the IN transfers magnetic flux to the network at a rate of 1.5×10^{24} Mx day^{-1} over the entire solar surface. This means that the IN supplies as much flux as is present in the network in only 9–13 hours, and could maintain it.

The results of Gošić et al. (2014) suggest that the IN is an important source of flux for the network, in agreement with the increasing evidence of a surface SSD contributing to the network field (Rempel 2014). On short-time scales, the IN flux transferred to the network may provide the seed for further amplification of the field up to kG values by convective collapse at the site of converging mesogranular and supergranular flows (Requerey et al. 2017, 2018), explaining the larger abundance of strong, long-lived flux concentrations in the network compared with the IN. This process would be consistent with the first mechanism of network formation described in Sect. 4.3.4.

To verify or refute this idea, an observational investigation of the appearance and evolution of magnetic flux in the network must be carried out, considering also the adjacent IN.

Particularly important is the site of appearance of new flux within the granulation pattern, as well as the interaction between network and IN fields, with a view to determine how the flux is eventually deposited in the network. Such an analysis has never been performed, although there exist observations with sufficient spatial resolution and sensitivity to detect weak magnetic flux appearing on subgranular scales (for example, the Hinode Solar Optical Telescope provides 0.3 arcsec and has a sensitivity of 10^{-3}, respectively).

2.5 Solar Cycle Variations of Quiet Sun Fields

Despite being plagued with difficulties, the search for possible variations of the quiet Sun magnetism with the solar cycle has been pursued vigorously in the last decades. This is because the detection of temporal and/or latitudinal variations would link the quiet Sun magnetism with the LSD responsible for the solar magnetic cycle. The main challenge is the need of very stable, homogeneous observations over periods of time spanning years. Few instruments are capable of providing such observations. Space-borne measurements are preferred, but also ground-based Hanle effect observations have been used to that end.

As summarized in Sect. 3.2 of Hinode Review Team et al. (2019), evidence for temporal variations of the polarization signals produced by quiet Sun fields is very marginal, if present at all. Most studies do not find significant changes or they are within the statistical uncertainties of the observations.

An analysis of 5.5 years of Hinode/SP data taken in quiet regions at the disk center revealed no measurable variation of either the magnetic flux or size distribution of IN patches with time (Buehler et al. 2013). Similar Hinode/SP observations were used to derive the transverse and longitudinal magnetic flux densities of very weak IN regions at different positions on the solar disk and study their variation from 2008 to 2015 (Jin and Wang 2015). No change in the flux density or the ratio of transverse to longitudinal flux was found. Following a different approach, synoptic Hinode/SP observations taken at various positions along the central meridian were used by Lites et al. (2014) to investigate the long-term evolution of the magnetic flux density in quiet IN regions. The transverse and unsigned longitudinal fluxes were found to be independent of the solar cycle at all solar latitudes, while the signed longitudinal fluxes (i.e., the polarity imbalance) showed clear changes in the polar regions and some hints of variation in the activity belt from 20 to 60 degrees latitude.

Full-disk observations in the near-infrared Fe I line at 1564.8 nm did not show notable changes in the properties of the polarization signals from IN regions for much of solar cycle 24 (Hanaoka and Sakurai 2020).

Faurobert and Ricort (2021) performed a Fourier analysis of the spatial fluctuations of the longitudinal flux density in small $10'' \times 10''$ IN regions along the central meridian, using synoptic data from the Hinode SP between 2008 and 2016. On scales smaller than $0.5''$ they did not find significant variations of the magnetic fluctuations with the solar cycle at any latitude. On granular scales, up to about $2.5''$, the power of the spatial fluctuations did not show variations at low and mid latitudes either, but a decrease was observed at high latitudes during solar maximum. The lack of changes on scales smaller than $0.5''$ indicates the presence of a time-independent magnetic field in the IN. However, the variation detected on larger scales at high latitude suggests that also the LSD contributes to the magnetism of the IN, although not homogeneously over the solar surface.

Using 12 years of SDO/HMI data, the rms longitudinal flux density in quiet $1^\circ \times 1^\circ$ IN regions at the central meridian was found to be nearly constant over time, with an average value of 6 Mx cm^{-2} (Korpi-Lagg et al. 2022). This was interpreted to reflect a real independence of the quiet IN magnetism on the solar activity cycle, or the inability of HMI to detect

changes due to insufficient sensitivity. By contrast, the rms flux density in 15° windows did show a statistically significant correlation with the solar cycle, with the maximum of the curve lagging the sunspot number cycle by about half a year. The difference is that these 15° windows contain both network and IN fields, whereas the 1° windows avoid the network fields. This suggests that the quiet network is indeed affected by the large-scale solar dynamo, although on supergranular timescales its evolution seems to be determined by interactions with IN fields, presumably reflecting a contribution from the SSD (see Sect. 2.4). Jin and Wang (2019) also found a variation of the network with the solar cycle using full-disk SDO/HMI magnetograms, but in this case the quiet network flux showed an anti-correlation with the sunspot number, due primarily to a reduction of the network area (the magnetic flux density of quiet network patches was observed to increase by about 6% at solar maximum). Further analyses are needed to clarify the exact variation of the quiet network with the sunspot cycle and the contribution of the SSD to its formation and maintenance.

Following a different strategy, the scattering polarization measurements of Kleint et al. (2010) did not show significant changes in the amount of Hanle depolarization of selected C_2 molecular lines over two years spanning the minimum phase of solar cycle 23. The observed lines are formed almost exclusively in granules, so they sample only the weakest fields of the quiet Sun. The latest analysis, covering almost a full solar cycle, still shows no clear changes in the Hanle depolarization with time (Ramelli et al. 2019). It is important to continue this type of synoptic Hanle programs and possibly extend them to the photospheric Sr I 460.7 nm line (which is formed also in the intergranular lanes), as they provide an independent way to examine the cycle dependence of the quiet Sun magnetism.

All these results point to no or little variations of the weak IN fields with the solar cycle, which supports the view that they are generated by an SSD and not by an LSD cascading down to smaller spatial scales. By contrast, the quiet network seems to show a variation with the solar cycle, indicating some contribution from the LSD in addition to a possible one from the SSD, but its amplitude and phase are not well determined yet.

2.6 Quiet Sun Chromospheric Fields

Compared with the photosphere, little is known about quiet Sun fields in the chromosphere. This is due to the very weak polarization signals they produce, the lack of spectropolarimetric observations with sufficient sensitivity to detect them, and the challenging interpretation of the measurements, which usually requires non-local thermodynamic equilibrium analyses (see the review by de la Cruz Rodríguez and van Noort 2017). However, some spectropolarimetric observations of quiet Sun fields have been made in the chromosphere, mainly to study how the longitudinal field changes with height in different magnetic structures (e.g., Gošić et al. 2018; Morosin et al. 2020; Esteban Pozuelo et al. 2023).

SSD action is not expected to occur at chromospheric heights due to the absence of turbulent flows, but there is an interest in understanding the influence on the chromosphere of quiet Sun fields generated deeper down. Network fields—whether produced by AR decay, ephemeral regions or IN fields—are essentially vertical and can reach the chromosphere and above, fanning out with height to form large-scale magnetic canopies. Most IN fields, on the contrary, seem to be low-lying structures confined to the photosphere (for an illustration, see the data-driven magnetofrictional simulations of Gošić et al. 2022). However, in some cases they manage to reach higher layers. Approximately 25% of the small-scale magnetic loops that emerge in the photosphere are observed to rise to chromospheric layers, producing localized brightenings and polarization signals there (Martínez González and Bellot Rubio 2009). These early results have recently been confirmed using full Stokes spectropolarimetry

at higher spatial resolution by Gošić et al. (2021), who reported the detection of circular polarization in the chromospheric Mg I b_2 517.3 and Ca II 854.2 nm lines produced by IN magnetic features ascending through the atmosphere.

These IN features may carry magnetic flux and energy to the chromosphere and so they have attracted much interest as a potential source of chromospheric heating in the quiet Sun (Ishikawa and Tsuneta 2009; Martínez González et al. 2010). The quiet Sun is particularly difficult to explain due to its continuous presence and large area coverage, which require a ubiquitous heating mechanism. Acoustic waves contribute to the heating, but their energy flux is not sufficient to explain the observed chromospheric emission (Fossum and Carlsson 2005; Molnar et al. 2023), hence the need to resort to mechanisms involving magnetic fields. The energy deposition triggered by IN features is probably caused by magnetic reconnection of the emerging field and pre-existing chromospheric fields, or reconnection of different chromospheric flux systems perturbed by the rising photospheric fields. Recently, it has been shown that the cancellation of IN fields can lead to local temperature enhancements of up to 2000 K in the low chromosphere (from $\log \tau_5 = -4$ to -6.5), explaining the appearance of strong brightenings at the position of the cancelling features (Gošić et al. 2018). However, the energy input estimated from the flux cancellation rates observed in these high-resolution observations falls short of being able to account for the quiet Sun chromospheric radiative losses, by an order of magnitude or so. If a large fraction of flux emergence and cancellation events go unnoticed because of the noise, then IN fields could still provide an important contribution to the heating of the chromosphere, but this needs to be confirmed with more sensitive spectropolarimetric measurements.

Another potential source of chromospheric heating involves the interaction of IN features and network fields described in Sect. 2.4. This interaction is detected observationally as continuous mergings and cancellations of magnetic flux at the edges of supergranular cells (Gošić et al. 2014). The reorganization of network field lines triggered by IN fields may be the source of the solar campfires recently discovered by Solar Orbiter. Campfires are small transient brightenings observed in EUV 17.4 nm images which have a tendency to occur at the edges of the photospheric network (Berghmans et al. 2021). The EUV campfires indicate transition region/coronal temperature enhancements and have been related to the cancellation of quiet Sun features (Panesar et al. 2021; Kahil et al. 2022), although in some cases no opposite-polarity fields could be detected at the location of the campfires. The origin of these features and their contribution to chromospheric/coronal heating are still being investigated, as several magnetic topologies leading to reconnection of field line bundles seem to be able to produce campfire-like events in simulations (Chen et al. 2021). Aspects of quiet-star chromospheres are covered in Sect. 5.2.

3 Basic Theoretical Concepts

We start our discussion about the theoretical and numerical studies of SSD with a short summary of the basic theoretical concepts. We then consider more idealized numerical models, used for studying the basic properties and parameter dependencies of SSD and comparisons with theory, and finally move on to surface convection simulations, which are calibrated and can be compared against observational data.

An SSD refers to the sustained and rapid amplification of magnetic field fluctuations at spatial scales smaller than the forcing scale in a plasma system. In the case of turbulent convection, the forcing scale is the scale at which the kinetic energy spectrum peaks, which is

the scale of convective cells, that is believed to vary strongly as function of depth: according to the mixing-length theory, the convective cells are small and turn over fast near the surface, and get progressively larger and slower as function of depth (Vitense 1953). The scale of convection is thought to behave this way because the convective bubbles moving up or downward are assumed to be able to travel a distance that is a fraction of the local pressure scale height, which decreases throughout the CZ, especially strongly near the surface. In the solar CZ, the plasma is turbulent enough to rapidly amplify magnetic fluctuations at or smaller than the scale of convective cells. The environment required for this dynamo instability to operate is such that the influence of rotation is weak and the flow is largely non-helical. This is in contrast to a LSD where the amplification of fields occurs at scales larger than the forcing scale, which is a consequence of symmetry breaking (due to helicity, inhomogeneities, anisotropies, etc.) at small scales, facilitating an inverse cascade of magnetic energy from small to large scales, further assisted by large-scale non-uniformities in the velocity field (see, e.g. Charbonneau 2020). This would suggest that the LSD would preferentially occur in the deeper layers of the CZ, where rotational influence on convection is strong, while SSD would operate nearly unimpeded in the surface layers, where the turbulent part of LSD would have only little chances of existing. As already hinted towards from observations, the situation is likely to be much more complex, with these two dynamo instabilities being excited together over a large fraction of the CZ, and non-linearly influencing each other.

Let us start our brief theoretical discussion by introducing the most important dimensionless control parameters of SSD-active systems. In the following, we use η for magnetic diffusivity, ν for kinematic viscosity and U as the typical velocity at the largest scale, L, of the inertial range. The latter also enters discussion of power spectra in terms of the scale of forcing/energy injections as $k_i \sim 1/L$. Then, the fluid Reynolds number is defined as $\mathrm{Re} = UL/\nu$ and the magnetic Reynolds number as $\mathrm{Re_M} = UL/\eta$. The magnetic Prandtl number is defined as the ratio of the two, namely $\mathrm{Pm} = \mathrm{Re_M}/\mathrm{Re}$, and can hence also be written as $\mathrm{Pm} = \nu/\eta$. The Reynolds numbers in the solar and stellar plasmas are both large, but the magnetic one is estimated, using the Spitzer formulae, to be a few orders of magnitude smaller than Re (see e.g., Brandenburg and Subramanian 2005). The solar Pm values are estimated to be in the range of 10^{-6} to 10^{-4} (see, e.g., Schumacher and Sreenivasan 2020), and the ones in even cooler stars even lower due to their increased density and lower interior temperatures.

Batchelor (1950) discussed the possibility of magnetic field amplification in a turbulent flow by drawing an analogy between the time evolution of vorticity in incompressible turbulence and the induction equation for the magnetic field. His model predicted no SSD for $\mathrm{Pm} < 1$ plasmas, however. The first rigorous mathematical treatment was performed by Kazantsev (1968), where it was shown that for the simple case of Gaussian zero-mean, homogeneous and isotropic velocity field that is δ-correlated in time (Kraichnan ensemble; Kraichnan 1968), the evolution of magnetic energy (or equivalently, the magnetic correlation tensor) can be expressed in a form similar to the Schrödinger equation with an effective "mass" and a "potential" that depends on the velocity correlation tensor. A description of this tensor then completes the system. The simplest assumption is to take the scale dependence of velocity fluctuations as $\langle \delta u(l) \rangle \sim l^{\alpha}$, where α can range from 0 to 1, corresponding to a "rough" and "smooth" velocity field, respectively. In the case of Kolmogorov turbulence (Kolmogorov 1941), $\alpha = 1/3$. The bound-state solutions of the equation, then, describe exponentially growing modes. When η is non-zero, this potential becomes repulsive at both the smallest and largest scales, allowing dynamo action to take place only if there is sufficient scale separation between the integral and the dissipative scales (see, e.g., Sect. 3.2 and

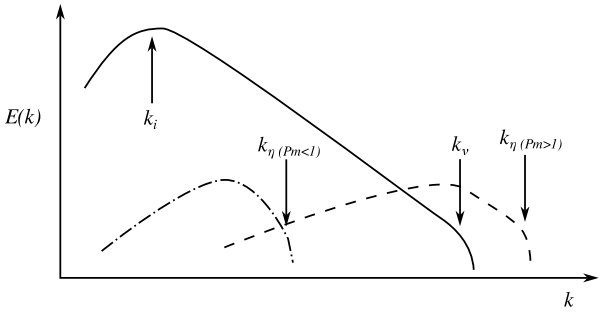

Fig. 6 Schematic of power spectrum for magnetic and kinetic energy in the low and high Pm regime. The solid line illustrates the kinetic energy for a turbulent plasma with energy injection at spatial wave number k_i and dissipation at k_ν. The dot-dashed (dashed) line show the magnetic energy power spectra in the kinematic growth phase with dissipation at scales $k_{\eta(\mathrm{Pm}<1)}$ ($k_{\eta(\mathrm{Pm}>1)}$) for the Pm < 1 (Pm > 1) case

Fig. 4 of Vincenzi (2001) for an illustration). In other words, there exists a critical magnetic Reynolds number $\mathrm{Re}_\mathrm{M}^\mathrm{crit}$ corresponding to this scale separation and dynamo action is possible only when $\mathrm{Re}_\mathrm{M} > \mathrm{Re}_\mathrm{M}^\mathrm{crit}$. This quantity depends on Re through Pm, the latter of which is independent of scales and flow properties.

According to Kazantsev's model, the amplification occurs at the timescale of the turbulent eddy turnover time, which is very short in comparison to the timescales required for the amplification of the large-scale field. In the kinematic growth phase, when the magnetic fluctuations are still weak, the structures generated have the thickness around the resistive scale, but are curved up to the scale of the turbulent eddies. Hence, the peak in the magnetic power spectrum is at the resistive scale, but all scales grow with the same growth rate. At scales larger than the resistive scale, a positive power law of $k \propto 3/2$ is predicted (Kazantsev 1968), hence called the Kazantsev spectrum, while at smaller scales, the spectrum can fall off very steeply, following the so-called Macdonald function (for details, see e.g. Brandenburg and Subramanian 2005; Rincon 2019).

In low-Pm plasmas, as the solar one, the resistivity, η, is much larger than the fluid viscosity, ν, meaning that the dissipation of the fluid motions occurs at scales much smaller than the scales at which magnetic fields dissipate (for an illustration of how the spatial power spectrum of magnetic and kinetic energy look like for low and high Pm cases, see Fig. 6). In effect, the turbulent eddies can dissipate into much smaller-scale structures than the magnetic structures, due to which the magnetic fluctuations must grow within the inertial range of the turbulent spectrum. The smoother magnetic structure, therefore, sees the turbulent eddies as a rough field around it (comparable to the "rough" flow in the Kazantsev picture); these circumstances are to be contrasted with high Pm fluids, where a smooth velocity field would be acting on smaller magnetic structures. The amplification of the magnetic fluctuation is more challenging in the former case of a rough velocity field, and hence the critical Reynolds number for dynamo action, $\mathrm{Re}_\mathrm{M}^\mathrm{crit}$, is elevated. At the incompressible limit or near it (weak compressibility), $\mathrm{Re}_\mathrm{M}^\mathrm{crit}$ ranges between 30–60 for high-Pm plasma (e.g., Brandenburg and Subramanian 2005), while for low Pm values of around 400 have been analytically computed (e.g., Kleeorin and Rogachevskii 2012).

How the SSD non-linearly saturates remains an open problem. Extending the analytical work on the Kazantsev model, it has been proposed that the SSD can grow magnetic fluctuations at the resistive scale up to and exceeding the equipartition with kinetic energy of turbulence, but that the generated field would be concentrated into resistive-scale ropes,

hence not being volume filling, and therefore being energetically rather insignificant (e.g. Subramanian 1998). The non-linear regime poses a formidable problem for analytical studies, but numerical studies can be attempted.

4 Numerical Models

Reaching the extreme-low Pms of the solar and stellar CZs is impossible currently and will most likely remain so in the future, at least for explicit-diffusion codes. The simulations conducted with these codes are also referred to as direct numerical simulations (DNS), although they are not quite fulfilling this definition in a strict sense, as orders of magnitude elevated diffusivities are used than in the real object; hence, hereafter we refer to these type of models as DNS-like.

An alternative to explicit diffusivity schemes is the usage of implicit large-eddy simulations (hereafter ILES), where the diffusive terms are replaced with numerical counterparts, providing diffusion only close to the grid scale, while leaving well-resolved scales unaffected. This has the advantage to maximize the Reynolds numbers in the flow. However, the actual values of the dimensionless control parameters then become ill-defined. There are various incarnations of these techniques, ranging from hyperviscous operators (see, e.g., Stein and Nordlund 1998) to slope-limited diffusion schemes (see, e.g., Rempel 2014), to mention just a couple (for a more thorough review, see Miesch et al. 2015).

Third type of numerical schemes are the so-called explicit large-eddy simulations (hereafter ELES), where the solved equations are filtered at a spatial scale larger than the grid scale, and (ideally) physically motivated subgrid-scale (SGS) models are used to describe the terms representing the scales left out by the filtering procedure. The best known example is the Smagorinsky scheme (Smagorinsky 1963), that develops a concept of turbulent eddy viscosity as an SGS model. More involved closures for the magnetized case, where more terms than the viscosity itself need to be described by the SGS model, have also been developed (see, e.g., Grete et al. 2017), although their usage in convection modeling is still limited. In the most complicated cases the ELES should also account for the influence of small-scale turbulence on large-scale dynamics, such as the inductive action of helical small-scale turbulence on large scales, dubbed the α effect, usually referred to as backscatter in LES terminology.

ILES schemes have been immensely successful for solar surface simulations with radiation transport (e.g. Stein and Nordlund 1998; Rempel 2014), as will be described later on in this chapter. However, concrete indications that ILES schemes might not be sufficient and appropriate for convective systems with LSD dynamo and SSD together come from comparisons like that of DNS-type simulations of Käpylä et al. (2017) and ILES-type ones of Hotta et al. (2016) showing markedly different behaviour (also to be discussed later in this chapter). Nevertheless, numerical models give valuable insights to the regimes where analytical approaches completely fail, such as studying the saturation mechanisms, and the interactions between SSD and LSD.

4.1 The Quest for Finding and Studying Low-Pm Small-Scale Dynamos

Numerical studies of SSD in solar and stellar contexts are challenging due to the low Pm of these environments. As discussed earlier, the critical $\mathrm{Re_M}$ required for the onset of SSD mechanism is expected to be in the order of hundreds, already requiring high resolution. But there is also the added challenge of Re required being orders of magnitude larger than $\mathrm{Re_M}$

to reach the physically relevant low-Pm regime. Hence, limited numerical studies exist with only moderately small Pm, with the minimal achieved values currently being approximately 0.003 by Warnecke et al. (2023). Only a fraction of studies pushing to the low-Pm regime include convection as the driver of the background turbulence, while the majority use some sort of idealized forcing function. It has been argued, however, that the SSD properties are only weakly dependent on the type of the forcing used (see, e.g., Moll et al. 2011). With the current computational resources we are, however, finally at the limit of being able to answer the first imminent question of whether the analytic predictions of $\mathrm{Re}_\mathrm{M}^\mathrm{crit}$ are correct, or if the threshold is lower/even higher than expected.

4.1.1 Kinematic Phase

While numerical evidence for SSD at $\mathrm{Pm} = 1$ in incompressible, homogeneous, isotropic, and non-helical setting was obtained several decades ago by Meneguzzi et al. (1981), and the literature of high-Pm number SSD in varying setups is abundant (see, e.g., the reviews by Brandenburg and Subramanian 2005; Rincon 2019), the first numerical evidence for low-Pm dynamos dates back to only 15 years (Iskakov et al. 2007). This initial evidence was restricted to simplified, forced, setups with hyperdiffusivity. The encouraging result from these studies is that the $\mathrm{Re}_\mathrm{M}^\mathrm{crit}$ does not continue increasing with Pm, but appears to have a maximum (Iskakov et al. 2007). A more recent DNS-like study by Warnecke et al. (2023) shows that after plateauing, $\mathrm{Re}_\mathrm{M}^\mathrm{crit}$ even starts decreasing again, approaching values of the order of a hundred. This non-monotonic behavior appears now to be firmly associated with the magnetic energy peak falling into the so-called bottleneck range of the kinetic spectrum (e.g. Brandenburg 2011; Warnecke et al. 2023). The bottleneck refers to both experimentally (reported in several papers since She and Jackson 1993) and numerically (reported since Dobler et al. 2003) confirmed inefficiency of the kinetic energy cascade at wavenumbers somewhat smaller than the viscous scale. This is seen most clearly by plotting the kinetic energy power spectrum (as in Fig. 6) compensated by $E(k)k^{5/3}$, which is the expected spectral kinetic energy cascade of the flow field for incompressible and homogeneous systems (Kolmogorov 1941), called the Kolmogorov law and cascade. For ideal Kolmogorov turbulence, it should result in a flat line in the inertial scale, followed by a drop-off around the viscous scale. However experiments and simulations show a "hump" that forms near the viscous scale before the drop-off occurs. This hump, especially when its lower wavenumber side, where the deviation from Kolmogorov scale is positive, overlaps with the energy-carrying scale wavenumber of the magnetic fluctuations, has been attributed to decreased SSD efficiency (Warnecke et al. 2023).

In the kinematic regime, one is additionally interested in determining the growth rate and its dependence on the key system parameters, and the evolution of the energy spectrum of the magnetic fluctuations, for which links to the Kazantzev theory can be established. Such links can be obtained by mapping an appropriate turbulence model, such as a one from Kolmogorov theory, to the Kazantsev theory. For example, the predicted growth rate by Kazantsev theory, $\gamma \propto u_\mathrm{d}/l_\mathrm{d}$, can be estimated by replacing estimates of dissipation scale velocity, u_d, and length scale, l_d, from Kolmogorov theory. Similarly, estimating $\mathrm{Re}_\mathrm{M}^\mathrm{crit}$ for different Pm has been based on using the roughness of the turbulent flow at different scales as a mapping (see, e.g., Boldyrev and Cattaneo 2004). Also, the effects of compressibility have been taken into account by assuming a linear relation between the transverse and the longitudinal component of the velocity correlation tensor for the two extreme cases of divergence-free (Kolmogorov turbulence) and irrotational (Burgers turbulence) flow and assuming the same form for the longitudinal component (see, e.g., Schober et al. 2012). For

solar-like weakly compressible flows all (semi-)analytical models indicate that a kinematic dynamo exists for the case of low Pm, and differ only in the details of the estimated $\mathrm{Re}_\mathrm{M}^\mathrm{crit}$ values for different flow fields.

The sparse set of numerical models so far indicate the following: for fixed Re_M, Schekochihin et al. (2007) reported growth rates monotonically decreasing with decreasing Pm (achieved through increasing Re) in the range $\mathrm{Pm} \approx 0.1$–1. For even smaller values, the growth rates were observed to tend towards a constant value. These findings led Schekochihin et al. (2007) to hypothesize that an asymptotic positive value of the growth rate would exist for high Re_M and low Pm values. However, such an asymptotic value has not been found yet, even for lower Pm studies (Warnecke et al. 2023). While, at $\mathrm{Pm} > 1$ regime, the growth rates retrieved from numerical experiments are closely consistent with the $\mathrm{Re}_\mathrm{M}^{1/2}$ scaling expected from Kolmogorov turbulence (reviewed, e.g., by Brandenburg and Subramanian 2005), the low-Pm simulations are less consistent with it (Iskakov et al. 2007; Schekochihin et al. 2007; Warnecke et al. 2023). A better match to a logarithmic scaling law, growth rate being proportional to $\ln\left(\mathrm{Re}_\mathrm{M}/\mathrm{Re}_\mathrm{M}^\mathrm{crit}\right)$, valid near the onset of the dynamo action (Kleeorin and Rogachevskii 2012), was reported by Warnecke et al. (2023). They concentrated on mapping the region near $\mathrm{Re}_\mathrm{M}^\mathrm{crit}$, hence this result might not be so unexpected. However, this also does not reveal the true scaling of growth rate, for which simulations far removed from $\mathrm{Re}_\mathrm{M}^\mathrm{crit}$ would be required. This is an extremely challenging task numerically.

As per the expected magnetic energy spectrum from Kazantsev theory, the simplified low-Pm models do not yield a direct agreement either (Iskakov et al. 2007; Schekochihin et al. 2007; Warnecke et al. 2023). Usually, for numerical convenience, the spectrum is cut short at low wavenumbers, so that the maximum range of higher wavenumbers could be modelled. Hence, in the setups trying to minimize Pm, the expected $k^{3/2}$ scaling of magnetic energy often cannot be seen by design. Nevertheless, at higher wavenumbers between the forcing and resistive scales, the magnetic spectra develop a cascade with negative power laws of varying steepness. Schekochihin et al. (2007) report spectral indices down to $-11/3$ at low Re_M and of -1 at higher Re_M, and Warnecke et al. (2023) find a slope approximately of -3 for their simulations near $\mathrm{Re}_\mathrm{M}^\mathrm{crit}$. As per as the visual appearance (see Fig. 7), the magnetic field exhibits less obvious folded structures having the width at the resistive scale, as would be expected from the Kazantsev model (Iskakov et al. 2007; Schekochihin et al. 2007; Warnecke et al. 2023). In the case of $\mathrm{Pm} = 1$ (left column, panels (a) and (c)), the correlation of magnetic field strength with high/low turbulent speeds is not very strong, while the magnetic field tends not to be volume filling. In the small Pm case (right column, panels (b) and (d)), the magnetic field has a clearly higher filling factor, and shows even a weaker correlation with the turbulent velocity field. Less folded and thicker structures are seen in the low-Pm case in comparison to Pm of unity.

With turbulent convection, SSD was established for $\mathrm{Pm} > 1$ simulations since the 1990s, the first successful convection simulation with self-sustaining magnetic fluctuations having been reported by Nordlund et al. (1992). Setups with Boussinesq approximation have been confirmed to exhibit SSD action (e.g., Cattaneo 1999), and the same applies also to stratified and compressible setups (e.g., Nordlund et al. 1992; Vögler and Schüssler 2007; Pietarila Graham et al. 2010; Hotta et al. 2015; Bekki et al. 2017).

Some attempts to go down to Pms of 0.1 have been performed in local stratified domains (Käpylä et al. 2018) in DNS-like deep convection setups, but no SSD action has been detected at the lower limit. In Käpylä et al. (2018) models, the growth and decay rates at variable Pm were found to be closely compatible with $\mathrm{Re}_\mathrm{M}^{1/2}$ scaling, which is different from the behavior seen in the simplified setups described above. Also, at small wavenumbers, the Kazantsev spectrum was not prominent, suggesting that the large-scale motions present in

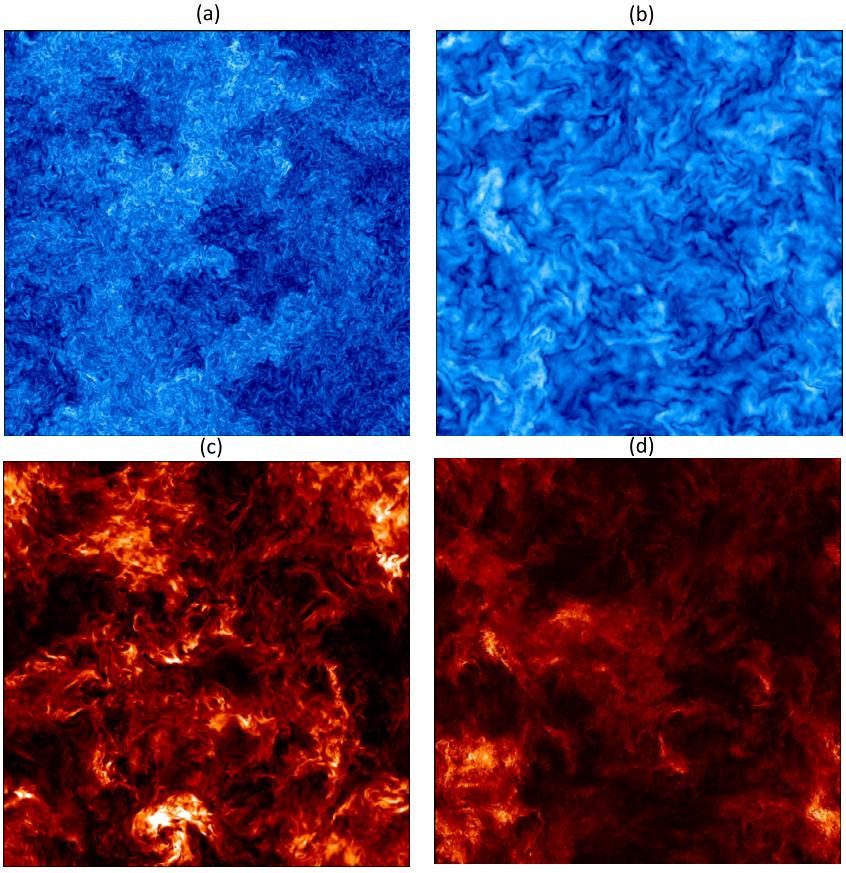

Fig. 7 Two-dimensional slices of the magnetic field strength (upper row) and speed (lower row), from $\mathrm{Pm} = 1$ simulation (left column) and $\mathrm{Pm} = 0.005$ (right column) simulations (reproduced from the models reported in Warnecke et al. 2023). The $\mathrm{Pm} = 1$ models were run with the resolution of 1024^3 and $\mathrm{Re} = \mathrm{Re_M} = 4096$, while the low Pm runs with the resolution of 4096^3, $\mathrm{Re} \approx 33{,}000$ and $\mathrm{Re_M} = 165$. In this model setup, the Reynolds numbers are defined using the forcing wavenumber, and are hence to be multiplied by 2π to match the definitions used in this paper. The simulation domain is fully periodic and has dimensions of $k_1 = 2\pi$ in all directions, while the white-in-time plane wave forcing has a mean wave number of $k_f = 2k_1$

the deep convection setups induce excess power to the magnetic energy spectrum. In models of solar surface convection with ILES schemes, however, SSD at around $\mathrm{Pm} \approx 0.1$ has been found (Rempel 2018; Brandenburg and Rempel 2019). In these works a low (numerical) Pm was realized by combining a more diffusive scheme for the induction equation with a less diffusive scheme for the momentum equation. The resulting effective (numerical) Pm was estimated from the solution based on the resulting effective diffusivities.

Global or semi-global convection simulations in spherical geometries have been reported to exhibit SSD, albeit still limited to $\mathrm{Pm} = 1$ regime (Hotta et al. 2016; Käpylä et al. 2017; Hotta and Kusano 2021). In such setups, rotation and stratification are included by default, raising the question whether the fluctuations are genuinely produced by SSD, or rather from a tangling of field generated from a LSD (see, e.g., the discussion in Brandenburg and Subramanian 2005). The most convincing experiments address this by removing the mean

field at each time step, hence allowing for the detection of SSD-generated fluctuations alone (for the method, see e.g. Käpylä et al. 2022).

In summary, at Pm $<$ 1, the numerical challenges have not yet enabled the detection of SSD in global models of turbulent convection. In the light of the evidence obtained from the more simplified systems, however, the earlier strong doubts about the existence of SSD in turbulent convection at low-Pm have recently been alleviated. Moreover, this question will be directly addressable in the near future with codes capable of taking advantage of accelerator platforms (see, e.g., Wright et al. 2021; Pekkilä et al. 2022).

4.1.2 Non-linear Saturation

Simulating low Pm SSD is an extremely challenging task from a computational power requirement perspective. The simultaneous requirement of high Re and an $\mathrm{Re_M} > \mathrm{Re_M^{crit}}$ for dynamo action requires extremely high resolutions and long integration times. Hence, even the most simplified setups operate in the kinematic regime, where the generated magnetic field has negligible back reaction on the flow. The non-linear regime of the SSD has been mainly studied for Pm $\geq$ 1, while only a handful of studies have been able to address the Pm $<$ 1 regime. Non-linear studies, however, are required to draw any conclusions on the effects of the SSD-generated fluctuations on the dynamics of systems like solar and stellar CZs, and about the interactions of the two dynamo instabilities (namely LSD and SSD).

The study of Brandenburg (2011) used DNS-like simulations to investigate SSD in forced non-helical turbulence in the non-linear regime adopting the following strategy. They ran a Pm $=$ 1 setup up to saturation, and then kept decreasing the kinematic viscosity while keeping $\mathrm{Re_M}$ roughly constant, and continuing the integration from the saturated state with the new parameter values. Their study led to two important findings. Firstly, most of the energy was found out to be dissipated via Joule heating before reaching to the viscous dissipation scale, hence allowing to decrease the kinematic viscosity even further than estimated for the specific grid resolution. Secondly, the saturation strength of the SSD was only weakly dependent on Pm, reducing from roughly 40 percent of equipartition with turbulence to near 10 percent when the Pm was changed by two orders of magnitude, when computed from volume-averages. However, at all scales, the magnetic energy was sub-dominant to the kinetic energy. Interestingly, the bottleneck effect, dominating the dynamics in the kinematic regime, was suppressed in the nonlinear regime. An attempt with a similar strategy with turbulent convection was undertaken by Käpylä et al. (2018), who found that the decrease of the saturation strength of the magnetic field was somewhat, but not detrimentally, stronger with Pm.

Brandenburg (2014) and Sahoo et al. (2011) performed further idealized simulations in the non-linear regime, reporting on the kinetic and magnetic dissipation rates, and their dependence on Pm. Brandenburg (2014) studied both helically and non-helically forced cases, the former also allowing for LSD. Interestingly, the ratio of kinetic to magnetic dissipation was observed to exhibit a positive power-law behaviour with Pm in both scenarios, albeit with somewhat varying power law index in helical versus non-helical cases. This implies that in the case of low-Pm dynamos the energy being pumped into the system through the kinetic energy reservoir (be it forcing, convection, shear, ...) is converted by the Lorentz force to magnetic energy more efficiently for smaller Pm, and then dissipated through resistive dissipation rather than through the viscous one.

At first sight these findings appear contradictory, how can the saturation field strength be mostly independent of Pm and the Lorentz force work vary strongly with Pm at the same time? Brandenburg and Rempel (2019) further studied the SSD saturation using both forced

DNS and convective ILES models and confirmed a similar behavior using both approaches. They further analyzed the transfer function of the Lorentz force in spectral space and found that there is a regime on small scales where the Lorentz force work can be positive, dubbed "reversed dynamo", as in the case of a normal dynamo, the flow is doing work against the Lorentz force, and a negative work contribution would be expected. The wavenumber at which this reversed dynamo regime is entered depends strongly on Pm. For a sufficiently low Pm the reversed dynamo is completely absent, but it is growing with increasing Pm until the positive energy transfer of the reversed dynamo on small scales almost completely offsets the negative transfer on large scales. As a consequence a high-Pm dynamo can have in the saturated state a strong field with little net Lorentz force work, while the transfer of energy from kinetic to magnetic energy on large scales remains strong. On small scales this energy is returned to kinetic energy and dissipated through viscosity. While the magnetic energy cascade extends to scales smaller than the kinetic energy cascade, there is very little energy left in that cascade. In the low-Pm regime the Lorentz force work is negative on all scales and most energy is dissipated through resistivity. While the kinetic energy cascade extends to much smaller scales, there is very little energy left in that cascade. As a consequence the saturated dynamo behaves in both cases like a $\mathrm{Pm} \sim 1$ dynamo since kinetic and magnetic energy cascades terminate at a similar scale, which is given by the larger of the viscous and resistive dissipation scales.

4.2 Models of Deep Convection

SSD action has not yet been found in DNS-like models of deep convection with low Pm. This is mostly due to lack of computing resources to properly investigate this regime. There is, however, rich literature and exciting findings at $\mathrm{Pm} \geq 1$ regime. This regime is either selected on purpose by using explicit viscosity schemes and setting $\nu \geq \eta$, or using ILES schemes, which results in effective Pms close to unity by inspecting the spectral cut-off scales.

SSD magnetic fields have been studied in local Cartesian convection setups, to maximize the fluid Reynolds numbers. In these studies Hotta et al. (2015, 2016), Bekki et al. (2017), an efficient SSD was found to operate, which also resulted in suppression of convective velocities near the base of the CZ. There, the magnetic and kinetic energies were found to be nearly in equipartition, resulting in the suppression of convective velocities by a factor of two relative to a purely hydrodynamic solution due to the Lorentz force feedback. The enthalpy flux was not, however, observed to be quenched thanks to a simultaneous suppression of horizontal mixing of entropy by the magnetic fluctuations. These results are suggestive of SSD aiding to resolve the convection conundrum by reducing the convective velocities while increasing the convective flux. The work of Karak et al. (2018), motivated by these results, studied cases of large thermal Prandtl numbers conjectured to be due to the suppression of thermal diffusion by the strong magnetic fluctuations. They could not provide support to these results, however. Therefore, as of writing of this chapter, the issue remains unresolved.

Global and semi-global simulations of solar and stellar magnetism have also recently reached parameter regimes where SSDs are obtained (Hotta et al. 2014, 2016; Käpylä et al. 2017; Hotta and Kusano 2021), but unless rotation is deliberately suppressed as in Hotta et al. (2014), LSD cannot be ruled out, and perhaps even then not completely, as anisotropies due to density stratification and inhomogeneties due to boundary conditions would still be present, giving a faint possibility of LSD to be excited.

All these models suggest that a vigorous SSD would have profound repercussions for the LSD and differential rotation, but the results appear rather divergent and dependent on

the viscosity schemes used. For example, Hotta et al. (2016) report on non-monotonic behavior of the LSD in the presence of SSD—at low resolution and Reynolds numbers with explicit diffusion scheme, the LSD and cyclic behavior is obtained, while it gets irregular and sub-critical at medium resolution, when switching to an ILES scheme. Increasing the resolution further, LSD is revived again, attaining saturation strengths larger than in the lowest resolution case. Whether this behavior is due to the change of the explicit/ILES schemes remains unclear, as no such non-monotonicity is observed when explicit schemes are used throughout (Käpylä et al. 2017).

Instead, Käpylä et al. (2017) report monotonically increasing values of the mean magnetic field, although the growth clearly slows down, and perhaps tends towards an asymptotic constant value. At the same time the differential rotation is strongly reduced. This can be traced back to the growing small-scale Maxwell stresses which oppose the small-scale Reynolds ones, and hence through that route lead to weaker differential rotation when the SSD becomes more vigorous. This could explain the tendency of the mean magnetic field growth slowing down as function of Re_M, hence reflecting only the quenching of the differential rotation rather than any asymptotics.

In the global magnetoconvection model of Hotta and Kusano (2021), on the other hand, increasing the resolution and consequently the Reynolds numbers to higher values than used before in similar type of ILES calculations, again at the effective $\mathrm{Pm} = 1$ limit, has been shown to lead to superequipartition of magnetic energy due to SSD at the small scales. This has been observed to result in more solar-like rotation profiles, meaning more radial than cylindrical isocontours of the angular velocity. In these computations, however, no LSD has yet been reported to be excited. This could be due to the difficulty of integrating long enough, albeit the simulations extend already up to 4000 days of solar evolution.

4.3 Development of Solar Surface Small-Scale Dynamo Simulations over the Past 2 Decades

Using an incompressible (Bousinesq) convective SSD simulation Cattaneo (1999) demonstrated that highly intermittent small-scale field with a saturation field strengths of about 20% equipartition (averaged over the simulation domain) could be reached in a stellar photosphere. This work suggested that substantial fraction of the quiet Sun magnetic field with strength of a few 10 G could originate from SSD action. Later Bercik et al. (2005) studied turbulent dynamos in solar like (F-M type) stars using anelastic simulations and found comparable results when applied to the Sun. Their work suggested that SSDs may explain the observed lower limits for X-ray fluxes from solar-like main sequence stars. This study is covered in more detail in Sect. 5. The first comprehensive SSD simulation of the solar photosphere (including compressibility, radiation transport, open bottom boundary conditions and an equation of state accounting for partial ionization) was presented by Vögler and Schüssler (2007). The simulation produced a mean vertical magnetic field amplitude of about 30 G in the photosphere and was subsequently compared in detail to observations through forward modeling of spectral lines using both Zeeman (Danilovic et al. 2010b) and Hanle (Shchukina and Trujillo Bueno 2011) diagnostics. It was found that these simulations fell short by a factor of 2–3 compared to Hinode observations of Zeeman polarisation in the Fe I 6302 Å lines; an even larger discrepancy by an order of magnitude was found comparing the Hanle depolarization in the Sr I 4607 Å line, suggesting that in addition to being too weak, the magnetic field was also falling off with height too rapidly. It was found by Rempel (2014) that increasing the resolution alone was insufficient to address the discrepancy. A critical component was to account for magnetic field that is transported into the photosphere from

the deeper layers of the CZ (see Sect. 4.3.1 for further detail). These improved simulations were again compared to observations through forward modeling (Danilovic et al. 2016a,b; del Pino Alemán et al. 2018) and it was found that simulations with a mean vertical field strength of around 60–80 G at optical depth unity in the photosphere were in agreement with constraints from both Zeeman and Hanle diagnostics. Khomenko et al. (2017) presented SSD simulations that included the Biermann Battery term (Biermann 1950) in the induction equation. It was found that this term produces at the edge of granules continuously seed fields with a strength of around 10^{-6} G, which can be amplified by the dynamo to saturation field strength within a few hours of time. While such fields are too weak to make a difference for the saturated dynamo state, this work highlights that fundamental physical processes do provide a lower bound for the quiet Sun magnetic field that is independent from external seeds (e.g. galactic magnetic field amplified during the star formation process).

4.3.1 Deep Versus Shallow Recirculation

A general challenge of near surface dynamo simulations is the treatment of the bottom boundary. Since closed boundary conditions enforce in the usually adopted shallow domains unphysical recirculation, most photospheric convection setups use bottom boundaries that are open for convective flows and mimic the presence of a deep CZ. Such an open bottom boundary does make SSD simulations ill-posed, since, dependent on the details of the boundary condition, magnetic energy can leave or enter the simulation domain. The work of Vögler and Schüssler (2007) used boundary conditions that do not allow for a Poynting flux at the bottom boundary in inflow regions. While downflows do transport energy out of the domain (owing to resistive transport right at the boundary), inflows do not transport energy back into the domain. This setup is conservative and demonstrates dynamo action in the presence of little local recirculation and continuous loss of magnetic energy towards the deep CZ, which was surmised to be a large hurdle for dynamo action in the photosphere (Stein et al. 2003). As descibed in Sect. 4.3 these models reached a vertical field strength of 30 G at optical depth unity, which is about a factor of 2–3 lower than implied by observations. The deeper parts of the solar convection have a larger magnetic Reynolds [Prandtl] numbers than the photosphere (10^9 [10^{-3}] instead of 10^5 [10^{-5}]), which should enable SSD action over a wide range of scales. Using ILES simulations Hotta et al. (2015) found super-equipartition fields near the base of the CZ in SSD simulations of the deep CZ. In addition, the deeper CZ will host magnetic field produced by the LSD, which may modulate the quiet Sun network field in addition as found in observations (Korpi-Lagg et al. 2022).

A fraction of this field is transported back to the surface and will appear in the photosphere and boost the amplification of field in the surface layers. Rempel (2014) captured this effect by allowing for the transport of horizontal field through the bottom boundary and by considering simulations with a closed boundary and complete recirculation and found and increase of the photospheric saturation field strength by about a factor of 2. Magnetic field that reaches the photosphere from deeper layers (deep recirculation) has undergone substantial horizontal expansion and appears as a rather smooth seed field in the center of granules, while magnetic field being brought back into the photosphere as a consequence of local downflow/upflow mixing (shallow recirculation) appears as a smaller-scale turbulent field at the edge of granules (Rempel 2018).

4.3.2 Energy Transfers, Saturation and Total Power of the Dynamo

Saturation of dynamo action at large magnetic Reynolds numbers is in general not a property of the velocity field, but rather about the relation of velocity and magnetic field to each other.

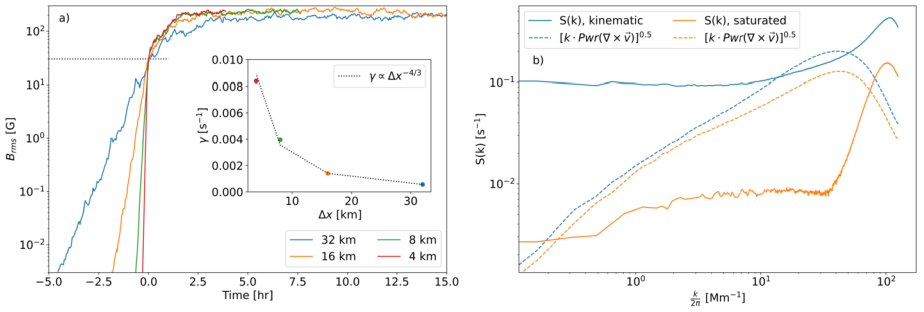

Fig. 8 Panel a): Transition from kinematic to saturated phase in ILES SSD simulations of the solar photosphere for models presented in Rempel (2014) with grid spacings from 32 down to 4 km. Presented is the time evolution of $B_{\rm rms}$ in the photosphere (optical depth of unity). All models start with the same seed field (around 0.001 G) and the curves are shifted such that the transition from kinematic to saturated phase lines up ($B_{\rm rms}$ of 30 G). The growth rate during the kinematic phase depends strongly on resolution as shown in the insert. Panel b): Saturation process of a ILES photospheric dynamo simulation. Shown are the effective shear rate (see text) and the vorticity spectrum during the kinematic and saturated phase

This was demonstrated by Tilgner and Brandenburg (2008), Cattaneo and Tobias (2009) for both small and LSD setups. They found that the velocity field of the saturated dynamo simulation remains to be an efficient growing dynamo in the kinematic regime, highlighting that saturation is not a property of the velocity field alone and requires a continuous adjustment of the velocity field to small changes in the saturated magnetic field solution.

Figure 8a) shows for various simulations from Rempel (2014) the transition from kinematic phase to saturated phase. We show here $B_{\rm rms}$ in the photosphere, which reaches in the saturated state values around 200–250 G, corresponding to about 30–40% of the equipartition value. While the models show large differences in the their kinematic growth rate depending on their resolution, after passing threshold of about $B_{\rm rms} = 30$ G, the remaining slow growth is similar and requires a few hours to reach the final saturation value. The saturation process was further studied in Rempel (2014) by looking at the effective shear rate defined in wavenumber space as

$$T_{MS}(k) = \frac{1}{8\pi} \hat{\vec{B}}(k) \cdot \widehat{[(\vec{B} \cdot \nabla)\vec{v}]}^{*}(k) + c.c. \tag{1}$$

$$E_M(k) = \frac{1}{8\pi} \hat{\vec{B}}(k) \cdot \hat{\vec{B}}^{*}(k) \tag{2}$$

$$S(k) = T_{MS}(k)/E_M(k) \tag{3}$$

During the kinematic growth phase $S(k)$ (Fig. 8b) has over a wide range of scales a value corresponding to the magnitude of vorticity (given by the quantity $\sqrt{k \cdot \mathrm{Pwr}(\nabla \times \vec{v})}$) on small scales. In the saturated state $S(k)$ has dropped over a wide range of scales by a factor of around 30 to values comparable to the magnitude of vorticity on the larges scales, while there is only a small reduction of the vorticity by less than a factor of 2 on the smallest scales. In the saturated state of the dynamo $S(k)$ is small due to combination a misalignment of the shear and magnetic field (reducing $(\vec{B} \cdot \nabla)\vec{v}$) and an induced field being mostly orthogonal to the existing field, minimizing the energy transfer while velocity shear remains mostly unchanged.

The growth rate of the ILES SSD shows in the explored range a very strong dependence on resolution (insert in Fig. 8a) in the form of $\gamma \propto (\Delta x)^{-4/3}$, which is significantly steeper

than the scaling of vorticity amplitude $\omega \sim k \cdot v \sim k^{2/3}$ (based on Kolmogorov scaling). For the case with 4 km grid spacing the growth rate for magnetic energy (twice the rate of $B_{\rm rms}$) is with 0.017 s^{-1} about 1/6 of the rate given by vorticity (Fig. 8b). It is currently uncertain how this scaling will change at higher resolution.

How much energy is required to maintain the small-scale magnetic field of the Sun? We can provide an estimate based on the previous discussion. With the small value of Pm $\sim 10^{-5}$ in the photosphere and values not much larger than 10^{-3} throughout the CZ, the dynamo is operating in a regime where the Lorentz force transfers energy from kinetic to magnetic energy on all scales and therefore maximises the power of the dynamo by minimising the energy lost to viscous dissipation. Rempel (2018) estimated from photospheric ILES dynamo simulations that about 150 erg cm^{-3} s^{-1} are available in the uppermost 1.5 Mm of the CZ to power the SSD, which is integrated over the whole solar surface about 30% of the solar luminosity. The total power of the SSD integrated over the volume of the CZ is bounded by the total pressure buoyancy driving, which is on the order of a few solar luminosities based on mixing length models. We note that the power of the dynamo can exceed a solar luminosity, since it is not a sink of energy. Through Ohmic dissipation this energy is returned to internal energy. If there would be no SSD a similar amount of energy would be dissipated through viscosity instead. Since the SSD alone is already capable of consuming most of the available convective driving, a LSD can only grow at the expense of the SSD as it has been suggested by Cattaneo and Tobias (2014). This would imply that the total power of the combined small- and LSD does not change much with rotation, while the structuring of magnetic field does change. Maintaining a magnetic field clumped into sunspots and starspots requires less energy than maintaining a field structured on the smallest scales, which maximises Ohmic dissipation. With a mean vertical magnetic field strength of around 60–80 G in the photosphere, the unsigned flux of the quiet Sun corresponds to about a 100 active regions at any given time. Reorganizing that amount of magnetic flux into starspots would turn the Sun into a very active star by comparison, while dramatically reducing Ohmic dissipation.

4.3.3 Anisotropy of Magnetic Field in Photosphere

As summarized in Sect. 2, observations indicate a significant anisotropy of the magnetic field above the photosphere in the sense that the horizontal field components are stronger than the vertical ones. The dynamo simulation of Vögler and Schüssler (2007) did show a similar preference for horizontal field as reported in Schüssler and Vögler (2008). It was found that at the height the Hinode lines are sensitive to, the strength of the horizontal field component is 4–5 times stronger than the vertical field component. Rempel (2014) analyzed SSD simulation in a wider and deeper domain that had the top boundary located about 1.5 Mm above the average $\tau_c = 1$ level. In these simulations it was found that the ratio of horizontal to vertical field peaks at a height of about 450 km (see Fig. 9). While the ratio of horizontal to vertical field reached values as high as 5 during the growth-phase of the dynamo, the ratio dropped to about 2.5 when the dynamo is saturated (Fig. 9a). Figure 9b) shows the strength of the vertical and horizontal field components individually. During the kinematic growth phase both drop monotonically with height, however, the vertical field component drops more rapidly with height, which leads to a peak in their ratio at around 450 km height. During the saturated phase the horizontal field strength does show a distinct peak, while the vertical field strength continues to drop monotonically. However, the magnitude of the magnetic field anisotropy is lower compared to the kinematic phase (a ratio of about 2.5 instead of 5).

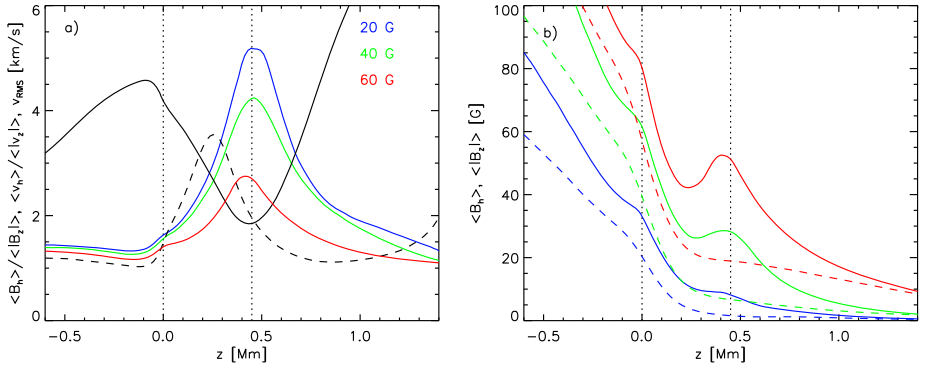

Fig. 9 Magnetic field anisotropy in upper CZ and photosphere. a): Ratio of horizontal to vertical field amplitude for 3 different field strengths (blue, green, red). The black solid line shows the convective RMS velocity, the black dashed line the velocity anisotropy. The peak of magnetic field anisotropy about 450 km above $\tau_c = 1$ coincides with the minimum of convective RMS velocity. b) Height variation of vertical (dashed) and horizontal (solid) field amplitudes. The fully saturated dynamo (red line) shows a distinct local peak of horizontal field amplitude at the location of minimum RMS velocity

What is the origin of the field anisotropy and specifically the origin of the peak in the horizontal field component? Obviously the velocity field is anisotropic above the granulation layer where overturning motions lead to preference of horizontal flows. However, the maximum flow field anisotropy is found at a height of about 250 km (black dashed line), which is 200 km lower than the height of peak anisotropy in the magnetic field. The height of peak field anisotropy does coincide with the minimum of the convective RMS velocity (black solid line). This in combination with the distinct peak in horizontal field strength may point to the diamagnetic part of turbulent pumping as the mechanism that expels horizontal magnetic field from the photosphere into lower chromosphere where it accumulates in the region with the lowest turbulence intensity. We note that this explanation is at best qualitative since SSD simulations do not have a large scale mean-field, however, the horizontal field overlying the photosphere is organized on scales larger than granules.

Alternative to the approach of using inversions to infer magnetic field anisotropy from observed Stokes profiles, this can also be achieved by analyzing the properties of the Stokes signals directly, specifically their center-to-limb variation. The simulation highlighted in Fig. 9 was compared to Hinode observations by Lites et al. (2017) and a good agreement between the CLV of synthetic and observed Stokes Q and U was found. This suggests that current photospheric SSD simulations do reproduce to a large extent the observed magnetic field anisotropy. A further test for these models would be multi-height observations that map out the amplitude of horizontal magnetic field in order to test the prediction of a peak in the horizontal magnetic field amplitude at a height of about 450 km.

4.3.4 Quiet Sun Network Field, Relevance for Coronal Heating

There are two common misconceptions: firstly, SSDs can only produce zero-mean fluctuations on the scale of granules and their downflow lanes, and secondly, that LSDs cannot produce zero-mean small-scale fluctuations through tangling of turbulent motions at the scale of convection. As a consequence both dynamos contribute to the organization of magnetic field on the observable scales from granules to super-granules. Here we focus specifically on the contribution from the SSD to network field.

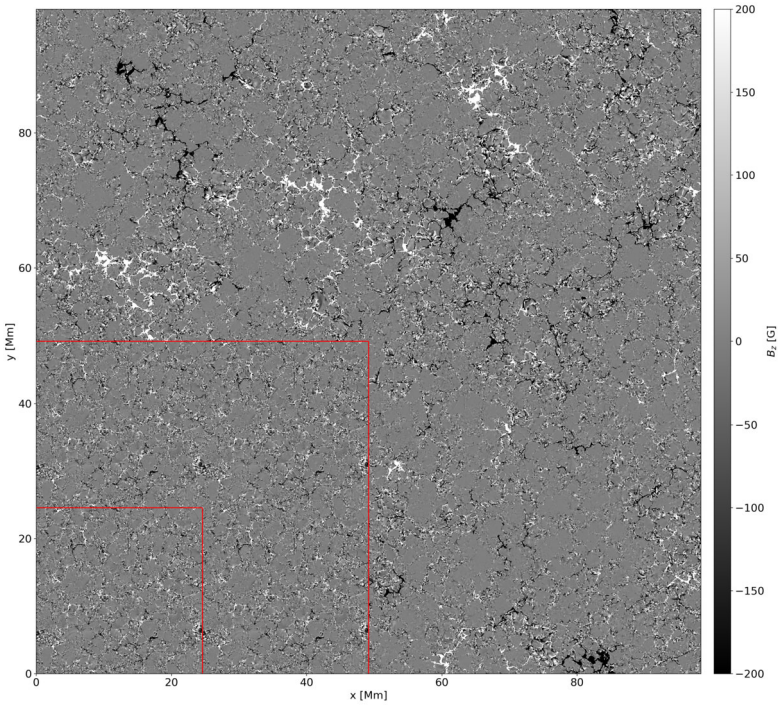

Fig. 10 Comparison of B_z at optical depth unity in two dynamo simulations with different domain sizes. The full horizontal extent shows results from a simulation in a $98.304 \times 98.304 \times 18.432$ Mm^3 domain. The small red box indicates a simulation in a $24.576 \times 24.576 \times 7.68$ Mm^3. For better visibility we periodically extended this simulation as a 2×2 tile (large red box). The SSD simulation in the wider and deeper domain does produce a mixed polarity network structure on scales larger than 10 Mm, which is absent in the smaller domain

Observations of the quiet Sun during a solar cycle minimum do show a quiet Sun mixed polarity network field (see, e.g., Fig. 13 in Lites et al. 2008), which raises the question of whether this network field is still a remnant of the LSD or if it is part of the quiet Sun and maintained by the SSD. Figure 10 compares 2 SSD simulations, one in a $98.304 \times 98.304 \times 18.432$ Mm^3 domain and one in a $24.576 \times 24.576 \times 7.68$ Mm^3 (see also Rempel 2014, 2020). Both simulations were set up with zero net flux on the scale of the simulation domain and both simulations have a mean vertical field strength of about 60 G. However, in the case of the wider and deeper simulation, we find larger scale flux imbalances that lead to the formation of network field. The larger simulation has on a scale of 24.576×24.576 Mm (extent of small simulation domain) an average flux imbalance corresponding to a mean vertical field of about 10 G. These flux imbalances are comparable to the imbalance found in the Hinode observations of Lites et al. (2008) (see Rempel (2020) for further discussion). These simulations suggest that the SSD does make at least a partial contribution to the quiet Sun network field, while at the same time there are also solar cycle dependent contributions from the LSD as found by Korpi-Lagg et al. (2022). We will discuss this further in Sect. 4.3.5 with regard to quiet Sun contributions to solar irradiance variations.

There are essentially two processes at work that lead to the emergence of a larger-scale network: (1) The dynamo is mostly saturated for the field strengths present in the solar photosphere. While the dynamo is very fast during the kinematic phase, simulations indicate

that the kinematic phase ends for field strengths that are about 10% of typical quiet Sun field strengths (see Fig. 8a). For stronger field the remaining growth time-scale is on the order of several hours, which means that the magnetic field can get organized by photospheric flows on scales larger than granulation. (2) As discussed in Sect. 4.3.1 at least 50% of the small-scale field present in the photosphere originates from deeper layers. In a deep, heavily stratified domain the field that is brought up from deeper layers is organized on scales of the deep seated, larger-scale convection and this organization is imprinted on the photosphere and further organized by (1). Further experiments (Rempel, 2022, private comm.) point towards (2) as the critical effect. Setups without deep recirculation (i.e. zero field in upflow regions at the bottom boundary) do not show a network structure even if deeper domains are used.

The quiet Sun network plays a critical role for shaping the upper solar atmosphere. Flux imbalance on larger-scales leads to stronger field reaching the corona, which is in turn critical for maintaining the quiet Sun corona. The need for a small flux imbalance (corresponding to about 5 G) was identified in models by Amari et al. (2015). Small-scale dynamo simulations in sufficiently deep domains with deep recirculation naturally produce such a flux imbalance on super-granular scales and have demonstrated that they can maintain a quiet Sun corona at temperatures in the 1–1.5 million K range (Rempel 2017; Chen et al. 2022).

4.3.5 Irradiance Properties of Quiet Sun Magnetic Field

While most small-scale magnetic fields in the quiet Sun are too weak to influence the radiative properties of the photosphere, simulations predict a small amount kG strength flux concentrations ($\lesssim$1%) in the photosphere which can enhance radiative losses similar to flux concentrations in solar network regions (regions of photosphere with a significant magnetic flux imbalance). As long as the quiet Sun can be considered as not varying (in the global sense) this will lead to an offset in the total and spectral solar irradiance (TSI/SSI) compared to a hypothetical non-magnetic Sun. However, if the quiet Sun varies over solar-cycle or even longer time-scales the quiet Sun magnetic field can make a contribution to the observed variation of TSI and SSI. We have to distinguish here between the network and the internetwork magnetic field. It is known from observations that quiet Sun network does have some residual variation with the cycle (Korpi-Lagg et al. 2022) on the order of 6 G, and has therefore contributions from both LSD and SSD. It is an open question whether the lowest level of quiet Sun network during the cycle minimum is a representation of the SSD contribution alone and therefore the lowest activity state possible or if a further drop of activity is possible. While observational support for a cycle variation of the internetwork field is marginal (see Sect. 2.5), we cannot rule it out completely. In order to assess the contribution of quiet Sun field it is necessary to derive the TSI or SSI sensitivity to changes of the quiet Sun field strength. This was investigated by Rempel (2020) who computed the TSI and SSI for quiet Sun (zero net flux) and weak network setups and found that a 7 G change of $\langle|B_z|\rangle$ on the $\tau_c = 1$ level (about 10% variation) causes about a 0.1% change in TSI. Given that this is about the total observed TSI change over the solar cycle and most of that is explained through contributions from the active Sun, there is very little room for the quiet Sun to vary over the solar cycle (meaning in addition to the quiet Sun network fraction that results from the LSD and is already considered in irradiance models). TSI provides more stringent constraints on quiet Sun variability than direct measurements of the magnetic field (see, e.g., Lites et al. 2014; Buehler et al. 2013; Meunier 2018; Faurobert and Ricort 2021). While this does not rule out longer-term variations of the quiet Sun, they are very unlikely to happen. The models from Rempel (2020) were used by Yeo et al. (2020) to reconstruct

solar TSI starting from HMI magnetograms (using radiative MHD simulations to translate HMI magnetograms into irradiance taking into account the full HMI data pipeline). It was found that 97% of the observed TSI variation can be accounted for that way, which gives a significant confidence that radiative MHD simulations capture the radiative properties of magnetic flux concentrations to a significant degree. Using this model they provided a lower bound for a grand minimum irradiance of no more than 2 W/m^2 lower than the 2019 solar cycle minimum. To this end SSD simulations were used to represent the lowest activity state of the Sun assuming that only the internetwork field is present. This is a lower bound, since as discussed in Sect. 4.3.4 a significant fraction of the network field present during a solar minimum could originate from a SSD and therefore would be part of the lowest possible activity state as well (i.e. present even during a grand minimum).

4.4 Radiative Zone

The SSD is usually understood to operate in the CZ, where the field is amplified by turbulent convection. However, no convection is possible in the stably-stratified radiative zones of stars. Does a source of turbulence still exist in these conditions, and does it have the required strength and properties to drive SSD? At the tachocline, shear instabilities, gravity waves as well as convective overshoot could, potentially, drive turbulence. Turbulence, in this case, is then no longer isotropic and comes under the realm of stably-stratified systems, an actively researched topic worth its own multiple review articles (see, e.g., Riley and Lindborg 2012; Lindborg 2006; Cheng et al. 2020, and references therein).

The essential feature of such turbulence is the existence of multiple scales over which the characteristics of turbulence change significantly. The length scales for the largest eddies in the vertical direction (with wavenumbers k_v) are much smaller than those in the horizontal direction (with wavenumber k_h), i.e., $k_v \gg k_h$. Apart from the usual Reynolds number, another dimensionless number enters into the picture: Froude number (Fr). This can be defined in the horizontal and vertical direction in terms of the Brunt-Väilsälä frequency N as $\mathrm{Fr}_h = Uk_h/N$, $\mathrm{Fr}_v = Uk_v/N$. Here, Fr_h can be understood as an inverse of the degree of stratification (in stably stratified system, $\mathrm{Fr}_h < 1$) and Fr_v can be understood as the ratio of inertial and buoyancy forces. Then there exists the Kolmogorov dissipation wave number $k_\nu \sim (\varepsilon/\eta^3)^{1/4}$ (Kolmogorov 1941) (where the kinetic energy gets dissipated), the Dougherty-Ozmidov wavenumber $k_O \sim (N^3/\varepsilon)^{1/2}$ (Dougherty 1961; Ozmidov 1965) (where energy in buoyant motions becomes comparable to the kinetic energy), and the buoyancy wavenumber $k_b \sim N/u$ (the length scale corresponding to the adiabatic displacement of a parcel with velocity u in the vertical direction). Under certain assumptions (Lindborg 2006), these wavenumbers (or, equivalently, length scales) can be described in terms of Re and Fr_h. In addition, in the presence of magnetic fields, there also exists the resistive wavenumber k_η (where magnetic energy gets dissipated).

The existence of SSD in solar radiative zone was investigated by Skoutnev et al. (2021) recently. In their paper, they consider a single $\mathrm{Fr} = u_{\mathrm{rms}}/l_i$, where $l_i \sim 1/k_i$ is the integral length scale. Hence, we shall use the same notation to describe their results. They considered 2 situations: i) $k_b < k_\nu < k_O$, ii) $k_b < k_O < k_\nu$, along with $k_\eta \lesseqgtr k_\nu$ for $\mathrm{Pm} \lesseqgtr 1$. In the first case, the small scale motions down to k_O are suppressed by viscosity making the flow more laminar and unsuitable for SSD growth. For the second case, however, Fr comes into the scaling. As $k_\nu \sim \mathrm{Re}^{3/4}\varepsilon^{-1/4}$ and $k_O \sim \varepsilon^{-1/2}\mathrm{Fr}^{-3/2}$, taking their ratio gives $k_\nu/k_O \sim (\mathrm{ReFr}^2)^{3/4}\varepsilon^{1/4}$. For fixed values of Pm, they explored the Re – Fr parameter space, and investigated the critical value of Re (Re^c) above which SSD action was possible. They found a scaling of $\mathrm{Re}^c \sim \mathrm{Fr}^{-2}$ for $\mathrm{Pm} \geq 1$, reducing the parameter space from Re – Fr – Pm

to Rb − Pm, where $\mathrm{Rb} = \mathrm{ReFr}^2$ is defined as a buoyancy Reynolds number. The two cases can then be distinguished as $\mathrm{Rb} < 1$ and $\mathrm{Rb} > 1$, respectively. Their main result was the existence of a critical Rb of around 3 to 9 (for high and low Pm regime, respectively) above which SSD action was possible. Since SSD fields are expected to be the fastest growing fields, these fields could influence the operation of instabilities associated with the generation of large-scale field at the base of the CZ (Spruit 1999). They also calculated the critical Rb from estimated solar values to be around a 100 (an order of magnitude higher than the critical value), which would imply that such a stably-stratified SSD could, in principle, exist in the solar interior. However, the sensitive dependence of this value on poorly constrained parameters like u, l_i for the solar interior makes this statement somewhat tentative.

5 SSD on Other Cool Stars

The Sun is the only star which we can resolve well enough to study detailed properties of granulation and quiet small-scale solar magnetism. For other stars the Zeeman-Doppler imaging inversion technique can be used to study their surface magnetic field (ZDI; see, e.g., Semel 1989). Due to the lack of surface resolution, this method has the capacity to trace the large-scale magnetic structures only. To estimate the total surface magnetic field, the Zeeman broadening and intensification can be used (see, e.g., Kochukhov et al. 2020). They demonstrated that only a fraction of the total magnetic field is recovered by ZDI. By combining ZDI with Zeeman broadening and intensification measurements, it is thus possible, in principle, to estimate how much of the magnetic field is hidden in small-scale structures (Trelles Arjona et al. 2021). Hence, it is well motivated to extrapolate our understanding of these phenomena to other stars similar to the Sun. In this review we consider the possible impact of this quiet star magnetism from the perspective of observations as well as theoretical modelling.

5.1 MHD Simulations of Near-Surface Stellar Convection

The first 3D MHD studies of SSD action in other stars, to the best of our knowledge, were conducted by Bercik et al. (2005). In this study, the authors consider anelastic simulations of near surface convection. The authors find the magnetic energy in the saturated phase of SSD evolution to be around 6.7% of the total kinetic energy. The X-ray and Mg II luminosities were then estimated by fitting the unsigned magnetic flux to empirical luminosity relations. This study, however, is anelastic and without proper radiative transfer, assumptions which fail near the surface. Despite these simplifications, a reasonable fit to the floor of X-ray and Mg II flux for cool main-sequence stars ranging in spectral class from F0 to M0 (Figs. 6 and 7) is reproduced, leading credence to the fact that SSD fields could, in principle, be responsible for lower limit of X-ray and chromospheric fluxes.

In addition, studies of fully compressible 3D MHD near-surface convection with realistic treatment of radiation have been conducted with varying strengths of imposed magnetic field, for example, by Beeck et al. (2015) using the MURaM code and Steiner et al. (2014) and Salhab et al. (2018) using the CO5BOLD code (Freytag et al. 2012). Since these studies have an imposed magnetic field, they cannot be considered quiet-star SSD simulations and are more comparable to a "plage" simulation, however, the weak field cases (20 G for the former, and 50 G for the latter) should provide an idea of the effect of effect of magnetic fields expected to arise from an SSD mechanism. The main takeaways from these simulations are that the small-scale magnetic flux concentrations form in the intergranular lanes

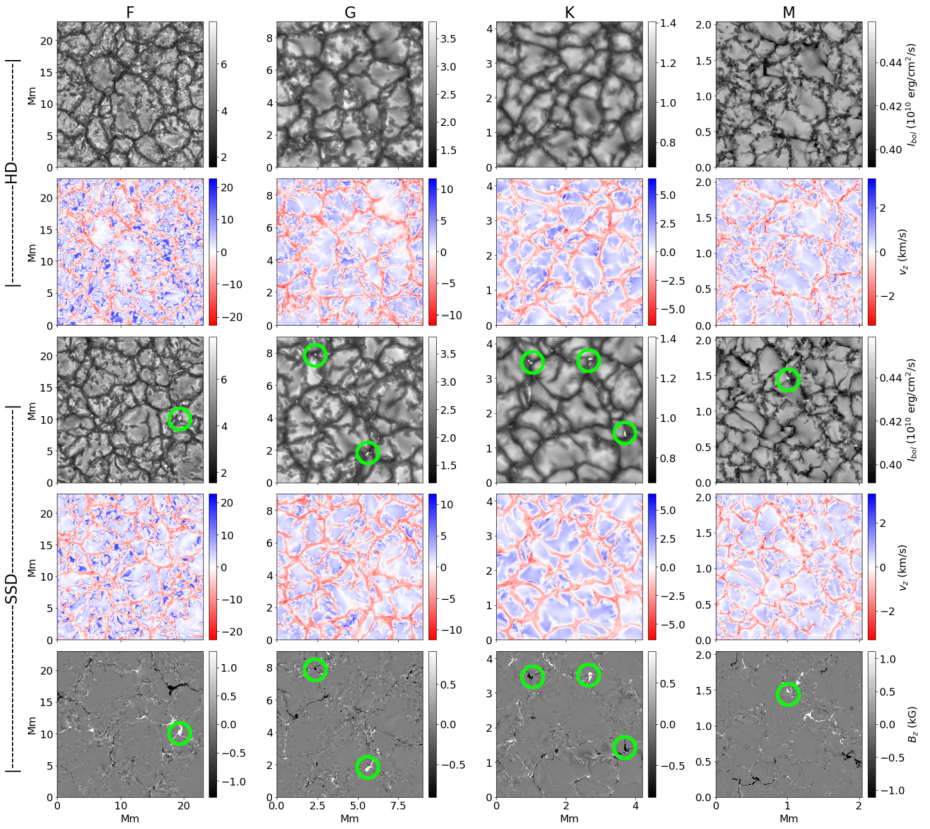

Fig. 11 Emergent intensity and surface vertical velocities in different stellar types for models with and without magnetic field. *From top to bottom:* Snapshot of the bolometric intensity and v_z at $\tau = 1$ for the hydrodynamic case (*row 1 and 2*), bolometric intensity and v_z at $\tau = 1$ for the SSD case (*row 3 and 4*) and the corresponding vertical magnetic field at $\tau = 1$ (*row 5, from left to right*) for spectral types F, G, K and M, respectively. The green circles indicate the bright points and corresponding magnetic field concentrations. Figure adapted from Bhatia et al. (2022)

with field values largely independent of stellar type at the $\tau = 1$ surface and that magnetic bright-points and filigree structure are apparent in the intergranular lanes, with highest contribution to bolometric intensity (at least for disk center) from around the G to K-type stars.

More recent simulations demonstrate that SSD action results in generation of magnetic fields of similar strength for all stars (F3V, G2V, K0V and M0V) considered (see Fig. 12, left panel; Bhatia et al. 2022) as well as reproduce the aforementioned features of magnetic field distribution (see Fig. 11 for a snapshot of said simulations). These simulations consist of two setups: one with self-consistently generated SSD fields with an open bottom boundary (same as *OSb* in Rempel 2014) and one that is purely hydrodynamic (HD). Compared to the pure HD runs, the SSD runs show small changes in the density and pressure stratification ($\sim$1%) for the F-star (Fig. 12, right panel), which is attributed to a decrease in turbulent pressure. This decrease in turbulent pressure occurs because the amplification of SSD fields takes away energy from the kinetic energy reservoir, decreasing the velocities (and, consequently, turbulent pressure). This effect is noticeable for the F-star because the kinetic energy is within an order of magnitude of the internal energy near the surface, whereas it is

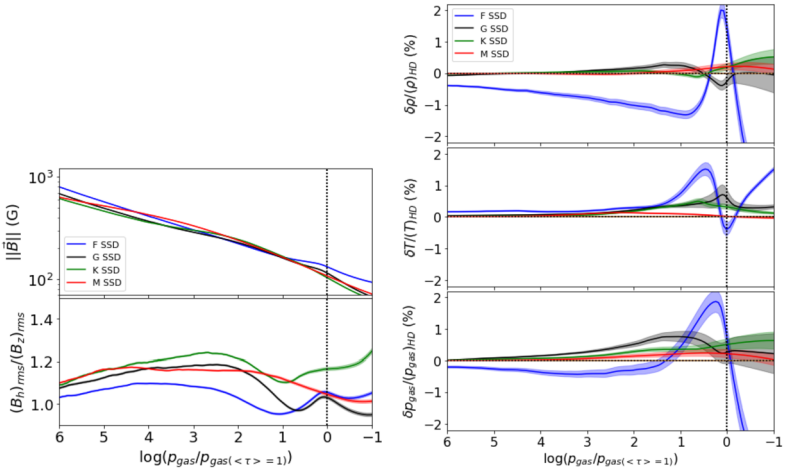

Fig. 12 *Left:* Horizontally averaged magnetic field magnitude (*top*) and the ratio of the horizontal r.m.s field strength to the vertical r.m.s field strength *bottom*. *Right:* Deviations in (*from top to bottom*) ρ, T and $p_{\rm gas}$ relative to hydrodynamic cases. The vertical axis gives the geometric deviations as a percentage relative to the hydrodynamic case. The horizontal axis is the number of pressure scale heights $\log_{10}(p_{\rm gas}/p_{{\rm gas}(\tau=1)})$, calculated for the HD cases, below the surface (*dotted vertical black line*). The shaded regions correspond to 1-σ standard error ($e = \sigma/\sqrt{N}$, N is the number of snapshots) computed over time averaging of snapshots. Figures adapted from Bhatia et al. (2022)

significantly smaller for other stars. At the photosphere, it is found that the effect of SSD fields is to reduce the upflow velocities for all cases, slightly decrease the average granule size for all cases and slightly increase the disk-center bolometric intensity for the G and K-star (Bhatia et al. 2023, submitted). The changes in velocity and intensity imply possible influence on high-resolution spectra. It must be noted that these simulations use gray radiative transfer (Rosseland mean opacities), so any analysis above the lower photosphere must be taken with a grain of salt. The authors are currently working on studies with 12-opacity bins, similar to what is used in Magic et al. (2015). In addition, these simulations have an effective Pm of $\sim$1.

5.2 Abundance Determination

The determination of stellar abundances is a vast field on its own, with applications ranging from planet formation and stellar evolution to cosmology (see, e.g., Jofré et al. 2019). The key ingredients to abundance determination are high resolution stellar spectra, precise atomic/molecular data and grids of model stellar atmospheres. As with other topics touched here, a complete discussion of these is well outside the scope of this article. Here, we focus on the last point regarding stellar models.

Traditionally 1D stellar models have been used to generate model spectra. However, these models rely on free parameters to model expected effects of convection (α mixing-length) and turbulence ($\eta_{\rm turb}$ microturbulent velocity). Asplund (2005) and Nissen and Gustafsson (2018) review the consequences for spectral line formation and abundance determination when effects of non-LTE and 3D convection are included in model atmospheres (see Sect. 2.3 of the first and Sect. 2.4 of the second reference, especially), and highlight the need for better models, especially for metal-poor stars. Section 2.6 of Nissen and Gustafsson (2018) also discusses the possible effect of SSD upon abundance determinations by

various authors (Fabbian et al. 2012; Shchukina and Trujillo Bueno 2015), with the broad picture being that the effect of SSD fields on abundance determinations is small and field-morphology dependent (with strong and organized field concentrations having the largest effect), but potentially non-negligible for stars other than the Sun. It must be noted that the spectral syntheses in these studies were carried out in LTE, and thus are not directly comparable to observations.

5.3 Basal Chromospheric Flux

Stellar chromospheres have historically been studied by considering activity indicators based on chromospheric emission lines, like the S-index (Baliunas et al. 1995). A review of stellar chromospheric activity is outside the scope of this article, and has been covered extensively elsewhere (e.g., Hall 2008; Linsky 2017; de Grijs and Kamath 2021, and references therein). The aspect of stellar chromospheric activity that concerns us is the minimum activity level or, equivalently, the basal chromospheric flux. Here we consider the term "basal" to refer to the minimum level of chromospheric activity that is independent of the stellar magnetic cycle.

For studies of stellar activity, the contribution from basal flux is usually estimated empirically from inactive stars (Mittag et al. 2013). This basal activity is color-dependent and was initially assumed to be due to acoustic heating (Schrijver 1987). The presence of a corona for solar-like "inactive" stars (Judge et al. 2004), as well as comparisons of observed solar chromospheric intensity fluctuations to models have brought this assumption into question (Fossum and Carlsson 2005). As described in Sect. 2.6, the current understanding is that acoustic waves alone are probably not sufficient to heat the chromosphere and that the magnetic field has an important role to play in the transport and dissipation of energy (Jefferies et al. 2006; Rajaguru et al. 2019). The precise details and mechanisms involved, however, remain poorly understood.

In the absence of sufficiently high-resolution observations, numerous simulations of the solar chromosphere illustrate the importance of magnetic fields in transferring energy to the chromosphere (see Sect. 5 of Carlsson et al. 2019, and references therein for an overview). Recent simulations of solar chromosphere using non-equilibrium ionization, non local-thermodynamic-equilibrium (Martínez-Sykora et al. 2019) indicated a dynamo-like process acting in the chromosphere converting kinetic to magnetic energy. Subsequent inclusion of ambiploar diffusion seems to, at least qualitatively, reproduce the observed Mg II emission line profiles (Martínez-Sykora et al. 2023). Current "realistic" simulations of the solar chromosphere using MURaM with a chromospheric extension (Przybylski et al. 2022) show that the net vertically directed Poynting flux at the base of the IN chromosphere (with fields generated from an SSD mechanism) provides sufficient energy (Withbroe and Noyes 1977) to heat the chromosphere (Przybylski, in prep.). In addition, these simulations seem to reproduce the observed Mg II line profiles significantly better than existing models (Ondratschek, in prep.). All of this recent progress in simulations of solar chromosphere, coupled with the fact the basal chromospheric flux is expected to be quite universal for stars with an outer CZ (Schröder et al. 2012), makes the prospect of modelling stellar chromospheres an achievable goal in the near future.

5.4 Stellar Variability and Exoplanet Detection

In the last two decades, the field of exoplanet detection has exploded. Dedicated exoplanet hunting missions like Kepler/K2, TESS and, soon, PLATO, in hand with follow-up radial velocity (RV) observations from ground-based echelle spectrometers like CARMENES (Quirrenbach et al. 2016) and ESPRESSO-VLT (the latter with resolving power over 190,000 in

the visible wavelength region; Pepe et al. 2021), have made it possible to detect and study rocky exoplanets (Pepe et al. 2013; Ribas et al. 2018). The instrumental precision of these modern spectrometers are within 10 cm/s, making it possible, in principle, to detect and characterize an earth-like planet orbiting around a Sun-like star (the RV contribution of the earth to the Sun is around 9 cm/s).

However, stellar variability remains the single largest source of uncertainty in current observations. The strategies commonly used to account for stellar variability at small timescales (granulation, p-mode oscillations, etc.) revolve around tweaking observation frequency and exposure times (Dumusque et al. 2011) to essentially average them out as best as possible. This can become prohibitively costly to approach noise level of less than 10 cm/s, as granulation is expected to be correlated for timescales much longer than few minutes (Meunier et al. 2015). Another approach is to model effects of stellar convection using realistic radiative-MHD simulations to model contributions of granulation to RV signal (Cegla et al. 2013). On the theoretical side, simulations of SSD in solar convection (Hotta et al. 2015), as well as near-surface convection for other cool main-sequence stars (Bhatia et al. 2022) have shown a consistent reduction in convective velocities. This reduction in convective velocities may be expected to influence the RV signal of granulation and characteristics of pressure modes.

In addition, the time-averaged stellar photospheric lines show a asymmetry due to granular motions, termed convective blueshift (Dravins 1987). This is one of the few observable signatures of stellar granulation and the degree of this blueshift for different spectral lines at different formation heights show a sort of universal scaling with effective temperature for different stellar types (Gray 2009; Liebing et al. 2021). Shporer and Brown (2011) showed using a simplified model how convective blueshift could influence the measurement of spin-orbit angles. Bhatia et al. (2023, submitted) show that in simulations of stellar photospheres with SSD fields, there is a reduction not only in convective velocities but also the scale of granulation (granules appear to be slightly smaller in presence of SSD fields), especially so for hotter spectral types.

Lastly, the center-to-limb variation of spectral intensities (used, among other things, for characterizing exoplanetary transits) is usually estimated from 1D model atmospheres. However, there have been discrepancies in comparison between true limb darkening from exoplanetary transit and model atmosphere based limb darkening (Howarth 2011), which could be accounted for by better models. Existing 3D hydrodynamic simulations already show a systematic difference in limb darkening calculated from 1D atmospheres (Magic et al. 2015). To improve precision of stellar photometry (important for determination of stellar radii as well as for transmission spectroscopy; de Wit and Seager 2013), it is necessary to account for these effects.

6 Outlook

Small-scale dynamo simulations that describe the process in solar and stellar CZs and photosphere require ingredients that go in several aspects beyond the simplified setups that are used to study the fundamentals of the dynamo processes, and their kinematic and non-linear phases, important in their own right. At a minimum, these setups require stratification and turbulence that is driven through convection, which results in the case of photospheric simulations from a volumetric cooling term based on radiative losses (typically computed from full 3D radiative transfer). Furthermore, the near surface layers of the Sun and Sun-like stars require an equation of state that accounts for the partial ionization of the most abundant

elements. Simulations of the photosphere of the Sun and Sun-like stars typically use rather shallow domains that do not reach to the base of the convective envelope and just capture the uppermost 5–10 density scale-heights. In such setups it is not uncommon to use an open lower boundary condition (allowing for vertical mass and convective energy flux) that mimics the deeper CZ. Such open boundary conditions lead to a less well determined dynamo problem, since solutions and their saturation will depend on the Poynting flux crossing the lower boundary, specifically the Poynting flux in upflow regions. Such dependence is not unphysical as it describes the not-directly-observable coupling between the photosphere and the deeper layers of the CZ. Ultimately it will be required to conduct SSD and LSD simulations in domains that reach from photosphere to the base of CZ to account for the full interaction of all convective scales in the system. Simulations that include all of the above listed ingredients are often referred as "realistic" or "comprehensive" simulations, however, their realism is, as in most simulations, determined by the affordable resolution, which limits the achievable Re and $\mathrm{Re_M}$ and typically constrains values of $\mathrm{Pm} = \mathrm{Re_M}/\mathrm{Re}$ close to unity. It is not uncommon for these models to use implicit large eddy simulations (ILES) in which diffusion terms are arising from the employed numerical scheme and are typically of a hyper-diffusive nature (higher order than Laplacian) with a non-linear dependence on the solution properties.

Although in simple cases ILES and DNS-type models do produce results that are in good agreement, they tend to disagree in situations where conditions for LSD onset are also fulfilled, that is, where rotation and its non-uniformities together with stratification are also allowed for. This seems to indicate that it does matter for the large-scale dynamics and magnetism how and at which scale the magnetic dissipation takes place, and investigating these issues further is an important future direction in deep convection models. LSD-SSD interactions cannot be ruled out as one decisive mechanism contributing to the convection conundrum and its solution.

The past couple of years have brought important verification steps of SSD excitation both in low-Pm and highly and stably stratified plasmas. While there is now nearly no doubt of the ubiquitous existence of SSD in solar and stellar convection and radiation zones, this raises the need of considering its role in various new scenarios, opening up new, exciting research avenues. However, in view of the drastic differences between $\mathrm{Pm} \approx 1$ systems and those with low Pm, albeit known mostly only in the kinematic regime, far-reaching conclusions from $\mathrm{Pm} = 1$ models should be avoided, and verification at lower Pm should always be pursued.

Solar observations will continue to play a critical role in constraining solar dynamo models. Of particular importance is to resolve the question of the isotropy of internetwork fields at different heights in the atmosphere and to study their temporal evolution from emergence until disappearance. The spatial distribution of the emergence sites in the granulation pattern may place additional constraints on the SSD mechanism and should be investigated further. DKIST will make it possible to tackle these questions with unprecedented sensitivity, providing precise linear polarization measurements over a much larger fraction of the solar surface than has been possible until now. DKIST will also obtain the first spatially and temporally resolved Hanle measurements ever, which will open new avenues for studying the weakest magnetic fields of the quiet solar photosphere. In order to allow for a comparison between simulations and observations we will need in the future higher resolution photospheric SSD simulations that also explore the low Pm regime present in the photosphere. At this point it is unknown if differences between the currently realized $\mathrm{Pm} \sim 1$ (ILES) simulations and the $\mathrm{Pm} \sim 10^{-5}$ regime of the solar photosphere will be detected or not.

Lastly, we note that SSD mechanism, as per the evidence presented in this review, is expected to be active across the HR diagram for all stars with a convective zone. The effects of

such a field on stellar atmospheres are only just beginning to be understood. Better models, together with some of the most precise instruments currently available for observations are pushing boundaries of not just detection and characterization of exoplanets but also detailed understanding of stellar structure and variability.

Acknowledgements MJKL acknowledges fruitful discussions with Dr. Jörn Warnecke and Dr. Thomas Hackman, and funding from the European Research Council (ERC) under the European Union's Horizon 2020 research and innovation program (Project UniSDyn, grant agreement no 818665). LBR acknowledges financial support from the Spanish MICIN/AEI 10.13039/501100011033 through grants RTI2018-096886-B-C5, PID2021-125325OB-C5, and PCI2022-135009-2, co-funded by "ERDF A way of making Europe", and through the "Center of Excellence Severo Ochoa" grant CEX2021-001131-S awarded to Instituto de Astrofísica de Andalucía. TB is grateful to Damein Przybylski for some great discussions on the role of magnetic fields in the solar chromosphere. This material is based upon work supported by the National Center for Atmospheric Research, which is a major facility sponsored by the National Science Foundation under Cooperative Agreement No. 1852977. MR received partial funding from NASA grant NNX17AI30G.

Author Contribution All authors contributed equally to this work.

Funding Note Open Access funding enabled and organized by Projekt DEAL.

Declarations

Competing Interests The authors declare no conflict of interests.

References

Abbett WP (2007) The magnetic connection between the convection zone and corona in the quiet Sun. Astrophys J 665(2):1469–1488. https://doi.org/10.1086/519788

Amari T, Luciani JF, Aly JJ (2015) Small-scale dynamo magnetism as the driver for heating the solar atmosphere. Nature 522(7555):188–191. https://doi.org/10.1038/nature14478

Asensio Ramos A (2009) Evidence for quasi-isotropic magnetic fields from Hinode quiet-Sun observations. Astrophys J 701(2):1032–1043. https://doi.org/10.1088/0004-637X/701/2/1032. arXiv:0906.4230 [astro-ph.SR]

Asensio Ramos A, Martínez González MJ (2014) Hierarchical analysis of the quiet-Sun magnetism. Astron Astrophys 572:A98. https://doi.org/10.1051/0004-6361/201423860. arXiv:1410.5953 [astro-ph.SR]

Asplund M (2005) New light on stellar abundance analyses: departures from LTE and homogeneity. Annu Rev Astron Astrophys 43(1):481–530. https://doi.org/10.1146/annurev.astro.42.053102.134001

Baliunas SL, Donahue RA, Soon WH et al (1995) Chromospheric variations in main-sequence stars. II. Astrophys J 438:269. https://doi.org/10.1086/175072

Batchelor GK (1950) On the spontaneous magnetic field in a conducting liquid in turbulent motion. Proc R Soc Lond Ser A 201(1066):405–416. https://doi.org/10.1098/rspa.1950.0069

Beck C, Rezaei R (2009) The magnetic flux of the quiet Sun internetwork as observed with the Tenerife infrared polarimeter. Astron Astrophys 502:969–979. https://doi.org/10.1051/0004-6361/200911727. arXiv:0903.3158

Beeck B, Schüssler M, Cameron RH et al (2015) Three-dimensional simulations of near-surface convection in main-sequence stars. III. The structure of small-scale magnetic flux concentrations. Astron Astrophys 581:A42. https://doi.org/10.1051/0004-6361/201525788. arXiv:1505.04739 [astro-ph.SR]

Bekki Y, Hotta H, Yokoyama T (2017) Convective velocity suppression via the enhancement of the subadiabatic layer: role of the effective Prandtl number. Astrophys J 851(2):74. https://doi.org/10.3847/1538-4357/aa9b7f. arXiv:1711.05960 [astro-ph.SR]
Bellot Rubio L, Orozco Suárez D (2019) Quiet Sun magnetic fields: an observational view. Living Rev Sol Phys 16(1):1. https://doi.org/10.1007/s41116-018-0017-1
Bellot Rubio LR, Orozco Suárez D (2012) Pervasive linear polarization signals in the quiet Sun. Astrophys J 757(1):19. https://doi.org/10.1088/0004-637X/757/1/19. arXiv:1207.0692 [astro-ph.SR]
Bercik DJ, Fisher GH, Johns-Krull CM et al (2005) Convective dynamos and the minimum X-ray flux in main-sequence stars. Astrophys J 631(1):529–539. https://doi.org/10.1086/432407. arXiv:astro-ph/0506027 [astro-ph]
Berghmans D, Auchère F, Long DM et al (2021) Extreme-UV quiet Sun brightenings observed by the Solar Orbiter/EUI. Astron Astrophys 656:L4. https://doi.org/10.1051/0004-6361/202140380. arXiv:2104.03382 [astro-ph.SR]
Bhatia TS, Cameron RH, Solanki SK et al (2022) Small-scale dynamo in cool stars. I. Changes in stratification and near-surface convection for main-sequence spectral types. Astron Astrophys 663:A166. https://doi.org/10.1051/0004-6361/202243607. arXiv:2206.00064 [astro-ph.SR]
Biermann L (1950) Über den Ursprung der Magnetfelder auf Sternen und im interstellaren Raum (mit einem Anhang von A. Schlüter). Z Naturforsch A 5(2):65–71. https://doi.org/10.1515/zna-1950-0201
Boldyrev S, Cattaneo F (2004) Magnetic-field generation in Kolmogorov turbulence. Phys Rev Lett 92(14):144501. https://doi.org/10.1103/PhysRevLett.92.144501. arXiv:astro-ph/0310780 [astro-ph]
Borrero JM, Kobel P (2011) Inferring the magnetic field vector in the quiet Sun. I. Photon noise and selection criteria. Astron Astrophys 527:A29. https://doi.org/10.1051/0004-6361/201015634. arXiv:1011.4380 [astro-ph.SR]
Borrero JM, Kobel P (2013) Inferring the magnetic field vector in the quiet Sun. III. Disk variation of the Stokes profiles and isotropism of the magnetic field. Astron Astrophys 550:A98. https://doi.org/10.1051/0004-6361/201118239. arXiv:1212.0788 [astro-ph.SR]
Brandenburg A (2011) Nonlinear small-scale dynamos at low magnetic Prandtl numbers. Astrophys J 741:92. https://doi.org/10.1088/0004-637X/741/2/92. arXiv:1106.5777 [astro-ph.SR]
Brandenburg A (2014) Magnetic Prandtl number dependence of the kinetic-to-magnetic dissipation ratio. Astrophys J 791:12. https://doi.org/10.1088/0004-637X/791/1/12. arXiv:1404.6964 [astro-ph.SR]
Brandenburg A, Rempel M (2019) Reversed dynamo at small scales and large magnetic Prandtl number. Astrophys J 879(1):57. https://doi.org/10.3847/1538-4357/ab24bd. arXiv:1903.11869 [astro-ph.SR]
Brandenburg A, Subramanian K (2005) Astrophysical magnetic fields and nonlinear dynamo theory. Phys Rep 417:1–209. https://doi.org/10.1016/j.physrep.2005.06.005. arXiv:astro-ph/0405052
Buehler D, Lagg A, Solanki SK (2013) Quiet Sun magnetic fields observed by Hinode: support for a local dynamo. Astron Astrophys 555:A33. https://doi.org/10.1051/0004-6361/201321152. arXiv:1307.0789 [astro-ph.SR]
Carlsson M, De Pontieu B, Hansteen VH (2019) New view of the solar chromosphere. Annu Rev Astron Astrophys 57:189–226. https://doi.org/10.1146/annurev-astro-081817-052044
Cattaneo F (1999) On the origin of magnetic fields in the quiet photosphere. Astrophys J Lett 515(1):L39–L42. https://doi.org/10.1086/311962
Cattaneo F, Tobias SM (2009) Dynamo properties of the turbulent velocity field of a saturated dynamo. J Fluid Mech 621:205. https://doi.org/10.1017/S0022112008004990
Cattaneo F, Tobias SM (2014) On large-scale dynamo action at high magnetic Reynolds number. Astrophys J 789(1):70. https://doi.org/10.1088/0004-637X/789/1/70. arXiv:1405.3071 [astro-ph.SR]
Cegla HM, Shelyag S, Watson CA et al (2013) Stellar surface magneto-convection as a source of astrophysical noise. I. Multi-component parameterization of absorption line profiles. Astrophys J 763(2):95. https://doi.org/10.1088/0004-637X/763/2/95. arXiv:1212.0236 [astro-ph.SR]
Centeno R, Socas-Navarro H, Lites B et al (2007) Emergence of small-scale magnetic loops in the quiet-Sun internetwork. Astrophys J Lett 666(2):L137–L140. https://doi.org/10.1086/521726. arXiv:0708.0844 [astro-ph]
Charbonneau P (2020) Dynamo models of the solar cycle. Living Rev Sol Phys 17(1):4. https://doi.org/10.1007/s41116-020-00025-6
Chen Y, Przybylski D, Peter H et al (2021) Transient small-scale brightenings in the quiet solar corona: a model for campfires observed with Solar Orbiter. Astron Astrophys 656:L7. https://doi.org/10.1051/0004-6361/202140638. arXiv:2104.10940 [astro-ph.SR]
Chen F, Rempel M, Fan Y (2022) A comprehensive radiative magnetohydrodynamics simulation of active region scale flux emergence from the convection zone to the corona. Astrophys J 937(2):91. https://doi.org/10.3847/1538-4357/ac8f95. arXiv:2106.14055 [astro-ph.SR]
Cheng Y, Li Q, Argentini S et al (2020) A model for turbulence spectra in the equilibrium range of the stable atmospheric boundary layer. J Geophys Res, Atmos 125(5):e2019JD032191. https://doi.org/10.1029/2019JD032191

Danilovic S, Beeck B, Pietarila A et al (2010a) Transverse component of the magnetic field in the solar photosphere observed by SUNRISE. Astrophys J Lett 723(2):L149–L153. https://doi.org/10.1088/2041-8205/723/2/L149. arXiv:1008.1535 [astro-ph.SR]

Danilovic S, Schüssler M, Solanki SK (2010b) Probing quiet Sun magnetism using MURaM simulations and Hinode/SP results: support for a local dynamo. Astron Astrophys 513:A1. https://doi.org/10.1051/0004-6361/200913379. arXiv:1001.2183 [astro-ph.SR]

Danilovic S, Rempel M, van Noort M et al (2016a) Observed and simulated power spectra of kinetic and magnetic energy retrieved with 2D inversions. Astron Astrophys 594:A103. https://doi.org/10.1051/0004-6361/201527917. arXiv:1607.06242 [astro-ph.SR]

Danilovic S, van Noort M, Rempel M (2016b) Internetwork magnetic field as revealed by two-dimensional inversions. Astron Astrophys 593:A93. https://doi.org/10.1051/0004-6361/201527842. arXiv:1607.00772 [astro-ph.SR]

de Grijs R, Kamath D (2021) Stellar chromospheric variability. Universe 7(11):440. https://doi.org/10.3390/universe7110440

de la Cruz Rodríguez J, van Noort M (2017) Radiative diagnostics in the solar photosphere and chromosphere. Space Sci Rev 210(1–4):109–143. https://doi.org/10.1007/s11214-016-0294-8. arXiv:1609.08324 [astro-ph.SR]

de Wit J, Seager S (2013) Constraining exoplanet mass from transmission spectroscopy. Science 342(6165):1473–1477

del Pino Alemán T, Trujillo Bueno J, Štěpán J et al (2018) A novel investigation of the small-scale magnetic activity of the quiet Sun via the hanle effect in the Sr I 4607 Å line. Astrophys J 863(2):164. https://doi.org/10.3847/1538-4357/aaceab. arXiv:1806.07293 [astro-ph.SR]

del Toro Iniesta JC, Ruiz Cobo B (2016) Inversion of the radiative transfer equation for polarized light. Living Rev Sol Phys 13:4. https://doi.org/10.1007/s41116-016-0005-2. arXiv:1610.10039 [astro-ph.SR]

Dobler W, Haugen NE, Yousef TA et al (2003) Bottleneck effect in three-dimensional turbulence simulations. Phys Rev E 68(2):026304. https://doi.org/10.1103/PhysRevE.68.026304. arXiv:astro-ph/0303324 [astro-ph]

Dougherty JP (1961) The anisotropy of turbulence at the meteor level. J Atmos Terr Phys 21(2):210–213. https://doi.org/10.1016/0021-9169(61)90116-7

Dravins D (1987) Stellar granulation. I – the observability of stellar photospheric convection. Astron Astrophys 172(1–2):200–224

Dumusque X, Udry S, Lovis C et al (2011) Planetary detection limits taking into account stellar noise. I. Observational strategies to reduce stellar oscillation and granulation effects. Astron Astrophys 525:A140. https://doi.org/10.1051/0004-6361/201014097. arXiv:1010.2616 [astro-ph.EP]

Esteban Pozuelo S, Asensio Ramos A, de la Cruz Rodríguez J et al (2023) Estimating the longitudinal magnetic field in the chromosphere of quiet-Sun magnetic concentrations. Astron Astrophys 672:A141. https://doi.org/10.1051/0004-6361/202245267. arXiv:2302.04258 [astro-ph.SR]

Fabbian D, Moreno-Insertis F, Khomenko E et al (2012) Solar Fe abundance and magnetic fields. Towards a consistent reference metallicity. Astron Astrophys 548:A35. https://doi.org/10.1051/0004-6361/201219335. arXiv:1209.2771 [astro-ph.SR]

Faurobert M, Ricort G (2021) Magnetic flux structuring of the quiet Sun internetwork. Center-to-limb analysis of solar-cycle variations. Astron Astrophys 651:A21. https://doi.org/10.1051/0004-6361/202140705. arXiv:2105.08657 [astro-ph.SR]

Fischer CE, Borrero JM, Bello González N et al (2019) Observations of solar small-scale magnetic fluxsheet emergence. Astron Astrophys 622:L12. https://doi.org/10.1051/0004-6361/201834628. arXiv:1901.05870 [astro-ph.SR]

Fischer CE, Vigeesh G, Lindner P et al (2020) Interaction of magnetic fields with a vortex tube at solar subgranular scale. Astrophys J Lett 903(1):L10. https://doi.org/10.3847/2041-8213/abbada. arXiv:2010.05577 [astro-ph.SR]

Fossum A, Carlsson M (2005) High-frequency acoustic waves are not sufficient to heat the solar chromosphere. Nature 435(7044):919–921. https://doi.org/10.1038/nature03695

Freytag B, Steffen M, Ludwig HG et al (2012) Simulations of stellar convection with CO5BOLD. J Comput Phys 231(3):919–959. https://doi.org/10.1016/j.jcp.2011.09.026. arXiv:1110.6844 [astro-ph.SR]

Gošić M (2015) The solar internetwork. PhD thesis, Universidad de Granada, Spain

Gošić M, Bellot Rubio LR, Orozco Suárez D et al (2014) The solar internetwork. I. Contribution to the network magnetic flux. Astrophys J 797(1):49. https://doi.org/10.1088/0004-637X/797/1/49. arXiv:1408.2369 [astro-ph.SR]

Gošić M, Bellot Rubio LR, del Toro Iniesta JC, Orozco Suárez D et al (2016) The solar internetwork. II. Flux appearance and disappearance rates. Astrophys J 820:35. https://doi.org/10.3847/0004-637X/820/1/35. arXiv:1602.05892 [astro-ph.SR]

Gošić M, de la Cruz Rodríguez J, De Pontieu B et al (2018) Chromospheric heating due to cancellation of quiet Sun internetwork fields. Astrophys J 857(1):48. https://doi.org/10.3847/1538-4357/aab1f0. arXiv:1802.07392 [astro-ph.SR]
Gošić M, De Pontieu B, Bellot Rubio LR, Sainz Dalda A et al (2021) Emergence of internetwork magnetic fields through the solar atmosphere. Astrophys J 911(1):41. https://doi.org/10.3847/1538-4357/abe7e0. arXiv:2103.02213 [astro-ph.SR]
Gošić M, Bellot Rubio LR, Cheung MCM, Orozco Suárez D et al (2022) The solar internetwork. III. Unipolar versus bipolar flux appearance. Astrophys J 925(2):188. https://doi.org/10.3847/1538-4357/ac37be. arXiv:2111.03208 [astro-ph.SR]
Gray DF (2009) The third signature of stellar granulation. Astrophys J 697(2):1032–1043. https://doi.org/10.1088/0004-637X/697/2/1032
Grete P, Vlaykov DG, Schmidt W et al (2017) Comparative statistics of selected subgrid-scale models in large-eddy simulations of decaying, supersonic magnetohydrodynamic turbulence. Phys Rev E 95(3):033206. https://doi.org/10.1103/PhysRevE.95.033206. arXiv:1703.00858 [physics.flu-dyn]
Hall JC (2008) Stellar chromospheric activity. Living Rev Sol Phys 5(1):2. https://doi.org/10.12942/lrsp-2008-2
Hanaoka Y, Sakurai T (2020) Internetwork magnetic fields seen in Fe I 1564.8 nm full-disk images. Astrophys J 904(1):63. https://doi.org/10.3847/1538-4357/abbc07. arXiv:2009.12751 [astro-ph.SR]
Hinode Review Team, Al-Janabi K Antolin P et al (2019) Achievements of Hinode in the first eleven years. Publ Astron Soc Jpn 71(5):R1. https://doi.org/10.1093/pasj/psz084
Hotta H, Kusano K (2021) Solar differential rotation reproduced with high-resolution simulation. Nat Astron 5:1100–1102. https://doi.org/10.1038/s41550-021-01459-0. arXiv:2109.06280 [astro-ph.SR]
Hotta H, Rempel M, Yokoyama T (2014) High-resolution calculations of the solar global convection with the reduced speed of sound technique. I. The structure of the convection and the magnetic field without the rotation. Astrophys J 786(1):24. https://doi.org/10.1088/0004-637X/786/1/24. arXiv:1402.5008 [astro-ph.SR]
Hotta H, Rempel M, Yokoyama T (2015) Efficient small-scale dynamo in the solar convection zone. Astrophys J 803(1):42. https://doi.org/10.1088/0004-637X/803/1/42. arXiv:1502.03846 [astro-ph.SR]
Hotta H, Rempel M, Yokoyama T (2016) Large-scale magnetic fields at high Reynolds numbers in magnetohydrodynamic simulations. Science 351(6280):1427–1430. https://doi.org/10.1126/science.aad1893. http://science.sciencemag.org/content/351/6280/1427
Howarth ID (2011) On stellar limb darkening and exoplanetary transits. Mon Not R Astron Soc 418(2):1165–1175. https://doi.org/10.1111/j.1365-2966.2011.19568.x. arXiv:1106.4659 [astro-ph.SR]
Ishikawa R, Tsuneta S (2009) Comparison of transient horizontal magnetic fields in a plage region and in the quiet Sun. Astron Astrophys 495(2):607–612. https://doi.org/10.1051/0004-6361:200810636. arXiv:0812.1631 [astro-ph]
Ishikawa R, Tsuneta S (2010) Spatial and temporal distributions of transient horizontal magnetic fields with deep exposure. Astrophys J Lett 718(2):L171–L175. https://doi.org/10.1088/2041-8205/718/2/L171. arXiv:1103.5812 [astro-ph.SR]
Ishikawa R, Tsuneta S (2011) The relationship between vertical and horizontal magnetic fields in the quiet Sun. Astrophys J 735(2):74. https://doi.org/10.1088/0004-637X/735/2/74. arXiv:1103.5556 [astro-ph.SR]
Iskakov AB, Schekochihin AA, Cowley SC et al (2007) Numerical demonstration of fluctuation dynamo at low magnetic Prandtl numbers. Phys Rev Lett 98(20):208501. https://doi.org/10.1103/PhysRevLett.98.208501. arXiv:astro-ph/0702291 [astro-ph]
Jefferies SM, McIntosh SW, Armstrong JD et al (2006) Magnetoacoustic portals and the basal heating of the solar chromosphere. Astrophys J Lett 648(2):L151–L155. https://doi.org/10.1086/508165
Jess DB, Jafarzadeh S, Keys PH et al (2023) Waves in the lower solar atmosphere: the dawn of next-generation solar telescopes. Living Rev Sol Phys 20(1):1. https://doi.org/10.1007/s41116-022-00035-6. arXiv:2212.09788 [astro-ph.SR]
Jin CL, Wang JX (2015) Does the variation of solar intra-network horizontal field follow sunspot cycle? Astrophys J 807(1):70. https://doi.org/10.1088/0004-637X/807/1/70
Jin CL, Wang JX (2019) Magnetic flux participation in solar surface magnetism during solar cycle 24. Res Astron Astrophys 19(5):069. https://doi.org/10.1088/1674-4527/19/5/69
Jin CL, Wang JX, Song Q et al (2011) The Sun's small-scale magnetic elements in solar cycle 23. Astrophys J 731:37. https://doi.org/10.1088/0004-637X/731/1/37. arXiv:1102.3728 [astro-ph.SR]
Jofré P, Heiter U, Soubiran C (2019) Accuracy and precision of industrial stellar abundances. Annu Rev Astron Astrophys 57:571–616. https://doi.org/10.1146/annurev-astro-091918-104509. arXiv:1811.08041 [astro-ph.SR]
Judge PG, Saar SH, Carlsson M et al (2004) A comparison of the outer atmosphere of the "flat activity" star τ Ceti (G8 V) with the Sun (G2 V) and α Centauri A (G2 V). Astrophys J 609(1):392–406. https://doi.org/10.1086/421044

Kahil F, Hirzberger J, Solanki SK et al (2022) The magnetic drivers of campfires seen by the Polarimetric and Helioseismic Imager (PHI) on Solar Orbiter. Astron Astrophys 660:A143. https://doi.org/10.1051/0004-6361/202142873. arXiv:2202.13859 [astro-ph.SR]
Käpylä PJ, Käpylä MJ, Olspert N et al (2017) Convection-driven spherical shell dynamos at varying Prandtl numbers. Astron Astrophys 599:A4. https://doi.org/10.1051/0004-6361/201628973. arXiv:1605.05885 [astro-ph.SR]
Käpylä PJ, Käpylä MJ, Brandenburg A (2018) Small-scale dynamos in simulations of stratified turbulent convection. Astron Nachr 339(127):127–133. https://doi.org/10.1002/asna.201813477. arXiv:1802.09607 [astro-ph.SR]
Käpylä MJ, Rheinhardt M, Brandenburg A (2022) Compressible test-field method and its application to shear dynamos. Astrophys J 932(1):8. https://doi.org/10.3847/1538-4357/ac5b78. arXiv:2106.01107 [physics.flu-dyn]
Karak BB, Miesch M, Bekki Y (2018) Consequences of high effective Prandtl number on solar differential rotation and convective velocity. Phys Fluids 30(4):046602. https://doi.org/10.1063/1.5022034. arXiv:1801.00560 [astro-ph.SR]
Kazantsev AP (1968) Enhancement of a magnetic field by a conducting fluid. Sov Phys JETP 26:1031
Khomenko EV, Collados M, Solanki SK et al (2003) Quiet-sun inter-network magnetic fields observed in the infrared. Astron Astrophys 408:1115–1135. https://doi.org/10.1051/0004-6361:20030604
Khomenko E, Vitas N, Collados M et al (2017) Numerical simulations of quiet Sun magnetic fields seeded by the Biermann battery. Astron Astrophys 604:A66. https://doi.org/10.1051/0004-6361/201630291. arXiv:1706.06037 [astro-ph.SR]
Kianfar S, Jafarzadeh S, Mirtorabi MT et al (2018) Linear polarization features in the quiet-Sun photosphere: structure and dynamics. Sol Phys 293(8):123. https://doi.org/10.1007/s11207-018-1341-2. arXiv:1807.04633 [astro-ph.SR]
Kleeorin N, Rogachevskii I (2012) Growth rate of small-scale dynamo at low magnetic Prandtl numbers. Phys Scr 86(1):018404. https://doi.org/10.1088/0031-8949/86/01/018404. arXiv:1112.3926 [astro-ph.SR]
Kleint L, Berdyugina SV, Shapiro AI et al (2010) Solar turbulent magnetic fields: surprisingly homogeneous distribution during the solar minimum. Astron Astrophys 524:A37. https://doi.org/10.1051/0004-6361/201015285
Kochukhov O, Hackman T, Lehtinen JJ et al (2020) Hidden magnetic fields of young suns. Astron Astrophys 635:A142. https://doi.org/10.1051/0004-6361/201937185. arXiv:2002.10469 [astro-ph.SR]
Kolmogorov A (1941) The local structure of turbulence in incompressible viscous fluid for very large Reynolds' numbers. Akad Nauk SSSR Dokl 30:301–305
Korpi-Lagg MJ, Korpi-Lagg A, Olspert N et al (2022) Solar-cycle variation of quiet-Sun magnetism and surface gravity oscillation mode. Astron Astrophys 665:A141. https://doi.org/10.1051/0004-6361/202243979. arXiv:2205.04419 [astro-ph.SR]
Kraichnan RH (1968) Small-scale structure of a scalar field convected by turbulence. Phys Fluids 11(5):945–953. https://doi.org/10.1063/1.1692063
Lamb DA, DeForest CE, Hagenaar HJ et al (2008) Solar magnetic tracking. II. The apparent unipolar origin of quiet-Sun flux. Astrophys J 674(1):520–529. https://doi.org/10.1086/524372
Liebing F, Jeffers SV, Reiners A et al (2021) Convective blueshift strengths of 810 F to M solar-type stars. Astron Astrophys 654:A168. https://doi.org/10.1051/0004-6361/202039607. arXiv:2108.03859 [astro-ph.SR]
Lindborg E (2006) The energy cascade in a strongly stratified fluid. J Fluid Mech 550:207–242. https://doi.org/10.1017/S0022112005008128
Linsky JL (2017) Stellar model chromospheres and spectroscopic diagnostics. Annu Rev Astron Astrophys 55(1):159–211. https://doi.org/10.1146/annurev-astro-091916-055327
Lites BW, Leka KD, Skumanich A et al (1996) Small-scale horizontal magnetic fields in the solar photosphere. Astrophys J 460:1019. https://doi.org/10.1086/177028
Lites BW, Kubo M, Socas-Navarro H et al (2008) The horizontal magnetic flux of the quiet-sun internetwork as observed with the hinode spectro-polarimeter. Astrophys J 672:1237–1253. https://doi.org/10.1086/522922
Lites BW, Centeno R, McIntosh SW (2014) The solar cycle dependence of the weak internetwork flux. Publ Astron Soc Jpn 66:S4. https://doi.org/10.1093/pasj/psu082
Lites BW, Rempel M, Borrero JM et al (2017) Are internetwork magnetic fields in the solar photosphere horizontal or vertical? Astrophys J 835(1):14. https://doi.org/10.3847/1538-4357/835/1/14
Magic Z, Chiavassa A, Collet R et al (2015) The STAGGER-grid: a grid of 3D stellar atmosphere models. IV. Limb darkening coefficients. Astron Astrophys 573:A90. https://doi.org/10.1051/0004-6361/201423804. arXiv:1403.3487 [astro-ph.SR]
Martínez González MJ, Bellot Rubio LR (2009) Emergence of small-scale magnetic loops through the quiet solar atmosphere. Astrophys J 700:1391–1403. https://doi.org/10.1088/0004-637X/700/2/1391. arXiv:0905.2691

Martínez González MJ, Collados M, Ruiz Cobo B et al (2007) Low-lying magnetic loops in the solar internetwork. Astron Astrophys 469:L39–L42. https://doi.org/10.1051/0004-6361:20077505. arXiv:0705.1319
Martínez González MJ, Manso Sainz R, Asensio Ramos A et al (2010) Small magnetic loops connecting the quiet surface and the hot outer atmosphere of the Sun. Astrophys J Lett 714(1):L94–L97. https://doi.org/10.1088/2041-8205/714/1/L94. arXiv:1003.1255 [astro-ph.SR]
Martínez González MJ, Manso Sainz R, Asensio Ramos A et al (2012) Dead calm areas in the very quiet Sun. Astrophys J 755(2):175. https://doi.org/10.1088/0004-637X/755/2/175. arXiv:1206.4545 [astro-ph.SR]
Martínez González MJ, Pastor Yabar A, Lagg A et al (2016) Inference of magnetic fields in the very quiet Sun. Astron Astrophys 596:A5. https://doi.org/10.1051/0004-6361/201628449. arXiv:1804.10089 [astro-ph.SR]
Martínez-Sykora J, Hansteen VH, Gudiksen B et al (2019) On the origin of the magnetic energy in the quiet solar chromosphere. Astrophys J 878(1):40. https://doi.org/10.3847/1538-4357/ab1f0b
Martínez-Sykora J, de la Cruz Rodríguez J, Gošić M et al (2023) Chromospheric heating from local magnetic growth and ambipolar diffusion under nonequilibrium conditions. Astrophys J Lett 943(2):L14. https://doi.org/10.3847/2041-8213/acafe9
Meneguzzi M, Frisch U, Pouquet A (1981) Helical and nonhelical turbulent dynamos. Phys Rev Lett 47(15):1060–1064. https://doi.org/10.1103/PhysRevLett.47.1060
Meunier N (2018) Solar chromospheric emission and magnetic structures from plages to intranetwork: contribution of the very quiet Sun. Astron Astrophys 615:A87. https://doi.org/10.1051/0004-6361/201730817. arXiv:1804.00869 [astro-ph.SR]
Meunier N, Lagrange AM, Borgniet S et al (2015) Using the Sun to estimate Earth-like planet detection capabilities. VI. Simulation of granulation and supergranulation radial velocity and photometric time series. Astron Astrophys 583:A118. https://doi.org/10.1051/0004-6361/201525721
Miesch M, Matthaeus W, Brandenburg A et al (2015) Large-Eddy simulations of magnetohydrodynamic turbulence in heliophysics and astrophysics. Space Sci Rev 194:97–137. https://doi.org/10.1007/s11214-015-0190-7. arXiv:1505.01808 [astro-ph.SR]
Milić I, Faurobert M (2012) Hanle diagnostics of weak solar magnetic fields: inversion of scattering polarization in c_2 and MGH molecular lines. Astron Astrophys 547:A38. https://doi.org/10.1051/0004-6361/201219737
Mittag M, Schmitt JHMM, Schröder KP (2013) Ca II H+K fluxes from S-indices of large samples: a reliable and consistent conversion based on PHOENIX model atmospheres. Astron Astrophys 549:A117. https://doi.org/10.1051/0004-6361/201219868
Moll R, Pietarila Graham J, Pratt J et al (2011) Universality of the small-scale dynamo mechanism. Astrophys J 736(1):36. https://doi.org/10.1088/0004-637X/736/1/36. arXiv:1105.0546 [astro-ph.SR]
Molnar ME, Reardon KP, Cranmer SR et al (2023) Constraining the systematics of (acoustic) wave heating estimates in the solar chromosphere. Astrophys J 945(2):154. https://doi.org/10.3847/1538-4357/acbc75. arXiv:2302.04253 [astro-ph.SR]
Moreno-Insertis F, Martinez-Sykora J, Hansteen VH et al (2018) Small-scale magnetic flux emergence in the quiet Sun. Astrophys J Lett 859(2):L26. https://doi.org/10.3847/2041-8213/aac648. arXiv:1806.00489 [astro-ph.SR]
Morosin R, de la Cruz Rodríguez J, Vissers GJM et al (2020) Stratification of canopy magnetic fields in a plage region. Constraints from a spatially-regularized weak-field approximation method. Astron Astrophys 642:A210. https://doi.org/10.1051/0004-6361/202038754. arXiv:2006.14487 [astro-ph.SR]
Nissen PE, Gustafsson B (2018) High-precision stellar abundances of the elements: methods and applications. Astron Astrophys Rev 26(1):6. https://doi.org/10.1007/s00159-018-0111-3. arXiv:1810.06535 [astro-ph.SR]
Nordlund A, Brandenburg A, Jennings RL et al (1992) Dynamo action in stratified convection with overshoot. Astrophys J 392:647. https://doi.org/10.1086/171465
Orozco Suárez D, Bellot Rubio LR (2012) Analysis of quiet-Sun internetwork magnetic fields based on linear polarization signals. Astrophys J 751(1):2. https://doi.org/10.1088/0004-637X/751/1/2. arXiv:1203.1440 [astro-ph.SR]
Orozco Suárez D, Katsukawa Y (2012) On the distribution of quiet-Sun magnetic fields at different heliocentric angles. Astrophys J 746(2):182. https://doi.org/10.1088/0004-637X/746/2/182
Orozco Suárez D, Bellot Rubio LR, del Toro Iniesta JC, Tsuneta S et al (2007) Quiet-Sun internetwork magnetic fields from the inversion of Hinode measurements. Astrophys J Lett 670(1):L61–L64. https://doi.org/10.1086/524139. arXiv:0710.1405 [astro-ph]
Orozco Suárez D, Bellot Rubio LR, del Toro Iniesta JC et al (2008) Magnetic field emergence in quiet Sun granules. Astron Astrophys 481:L33–L36. https://doi.org/10.1051/0004-6361:20079032. arXiv:0712.2663
Ozmidov RV (1965) On the turbulent exchange in a stably stratified ocean. Izv Acad Sci USSR Atmos Ocean Phys 1:861–871

Panesar NK, Tiwari SK, Berghmans D et al (2021) The magnetic origin of solar campfires. Astrophys J Lett 921(1):L20. https://doi.org/10.3847/2041-8213/ac3007. arXiv:2110.06846 [astro-ph.SR]
Pekkilä J, Väisälä MS, Käpylä MJ et al (2022) Scalable communication for high-order stencil computations using cuda-aware MPI. Parallel Comput 111:102904. https://doi.org/10.1016/j.parco.2022.102904
Pepe F, Cameron AC, Latham DW et al (2013) An Earth-sized planet with an Earth-like density. Nature 503(7476):377–380. https://doi.org/10.1038/nature12768. arXiv:1310.7987 [astro-ph.EP]
Pepe F, Cristiani S, Rebolo R et al (2021) ESPRESSO at VLT. On-sky performance and first results. Astron Astrophys 645:A96. https://doi.org/10.1051/0004-6361/202038306. arXiv:2010.00316 [astro-ph.IM]
Petrovay K, Szakaly G (1993) The origin of intranetwork fields: a small-scale solar dynamo. Astron Astrophys 274:543
Pietarila Graham J, Cameron R, Schüssler M (2010) Turbulent small-scale dynamo action in solar surface simulations. Astrophys J 714(2):1606–1616. https://doi.org/10.1088/0004-637X/714/2/1606. arXiv:1002.2750 [astro-ph.SR]
Przybylski D, Cameron R, Solanki SK et al (2022) Chromospheric extension of the MURaM code. Astron Astrophys 664:A91. https://doi.org/10.1051/0004-6361/202141230. arXiv:2204.03126 [astro-ph.SR]
Quintero Noda C, Schlichenmaier R, Bellot Rubio LR, Löfdahl MG et al (2022) The European Solar Telescope. Astron Astrophys 666:A21. https://doi.org/10.1051/0004-6361/202243867. arXiv:2207.10905 [astro-ph.SR]
Quirrenbach A, Amado PJ, Caballero JA et al (2016) CARMENES: an overview six months after first light. In: Evans CJ, Simard L, Takami H (eds) Ground-based and airborne instrumentation for astronomy VI. Proc SPIE 9908, p 990812. https://doi.org/10.1117/12.2231880
Rajaguru SP, Sangeetha CR, Tripathi D (2019) Magnetic fields and the supply of low-frequency acoustic wave energy to the solar chromosphere. Astrophys J 871(2):155. https://doi.org/10.3847/1538-4357/aaf883
Ramelli R, Bianda M, Berdyugina S et al (2019) Measurement of the evolution of the magnetic field of the quiet photosphere over a solar cycle. In: Belluzzi L, Casini R, Romoli M et al (eds) Solar polariation workshop 8, p 283
Rempel M (2014) Numerical simulations of quiet Sun magnetism: on the contribution from a small-scale dynamo. Astrophys J 789(2):132. https://doi.org/10.1088/0004-637X/789/2/132. arXiv:1405.6814 [astro-ph.SR]
Rempel M (2017) Extension of the MURaM radiative MHD code for coronal simulations. Astrophys J 834(1):10. https://doi.org/10.3847/1538-4357/834/1/10. arXiv:1609.09818 [astro-ph.SR]
Rempel M (2018) Small-scale dynamo simulations: magnetic field amplification in exploding granules and the role of deep and shallow recirculation. Astrophys J 859(2):161. https://doi.org/10.3847/1538-4357/aabba0. arXiv:1805.08390 [astro-ph.SR]
Rempel M (2020) On the contribution of quiet-Sun magnetism to solar irradiance variations: constraints on quiet-Sun variability and grand-minimum scenarios. Astrophys J 894(2):140. https://doi.org/10.3847/1538-4357/ab8633. arXiv:2004.01795 [astro-ph.SR]
Requerey IS, Del Toro Iniesta JC, Bellot Rubio LR et al (2017) Convectively driven sinks and magnetic fields in the quiet-Sun. Astrophys J Suppl Ser 229(1):14. https://doi.org/10.3847/1538-4365/229/1/14. arXiv:1610.07622 [astro-ph.SR]
Requerey IS, Cobo BR, Gošić M et al (2018) Persistent magnetic vortex flow at a supergranular vertex. Astron Astrophys 610:A84. https://doi.org/10.1051/0004-6361/201731842. arXiv:1712.01510 [astro-ph.SR]
Ribas I, Tuomi M, Reiners A et al (2018) A candidate super-Earth planet orbiting near the snow line of Barnard's star. Nature 563(7731):365–368. https://doi.org/10.1038/s41586-018-0677-y. arXiv:1811.05955 [astro-ph.EP]
Riley JJ, Lindborg E (2012) Recent progress in stratified turbulence. Cambridge University Press, Cambridge. https://doi.org/10.1017/CBO9781139032810.008
Rimmele TR, Warner M, Keil SL et al (2020) The Daniel K. Inouye Solar Telescope – observatory overview. Sol Phys 295(12):172. https://doi.org/10.1007/s11207-020-01736-7
Rincon F (2019) Dynamo theories. J Plasma Phys 85(4):205850401. https://doi.org/10.1017/S0022377819000539. arXiv:1903.07829 [physics.plasm-ph]
Sahoo G, Perlekar P, Pandit R (2011) Systematics of the magnetic-Prandtl-number dependence of homogeneous, isotropic magnetohydrodynamic turbulence. New J Phys 13(1):013036. https://doi.org/10.1088/1367-2630/13/1/013036. arXiv:1006.5585 [nlin.CD]
Salhab RG, Steiner O, Berdyugina SV et al (2018) Simulation of the small-scale magnetism in main-sequence stellar atmospheres. Astron Astrophys 614:A78. https://doi.org/10.1051/0004-6361/201731945
Schekochihin AA, Iskakov AB, Cowley SC et al (2007) Fluctuation dynamo and turbulent induction at low magnetic Prandtl numbers. New J Phys 9(8):300. https://doi.org/10.1088/1367-2630/9/8/300. arXiv:0704.2002 [physics.flu-dyn]
Schober J, Schleicher D, Bovino S et al (2012) Small-scale dynamo at low magnetic Prandtl numbers. Phys Rev E 86(6):066412. https://doi.org/10.1103/PhysRevE.86.066412. arXiv:1212.5979 [astro-ph.CO]

Schrijver CJ (1987) Magnetic structure in cool stars. XI. Relations between radiative fluxes mesuring stellar activity, and evidence for two components in stellar chromospheres. Astron Astrophys 172:111–123
Schrijver CJ, Harvey KL (1994) The photospheric magnetic flux budget. Sol Phys 150:1–18. https://doi.org/10.1007/BF00712873
Schröder KP, Mittag M, Pérez Martínez MI et al (2012) Basal chromospheric flux and Maunder minimum-type stars: the quiet-Sun chromosphere as a universal phenomenon. Astron Astrophys 540:A130. https://doi.org/10.1051/0004-6361/201118363. arXiv:1202.3314 [astro-ph.SR]
Schumacher J, Sreenivasan KR (2020) Colloquium: unusual dynamics of convection in the Sun. Rev Mod Phys 92(4):041001. https://doi.org/10.1103/RevModPhys.92.041001
Schüssler M, Vögler A (2008) Strong horizontal photospheric magnetic field in a surface dynamo simulation. Astron Astrophys 481:L5–L8. https://doi.org/10.1051/0004-6361:20078998. arXiv:0801.1250
Semel M (1989) Zeeman-Doppler imaging of active stars. I – basic principles. Astron Astrophys 225:456–466
Shchukina N, Trujillo Bueno J (2011) Determining the magnetization of the quiet Sun photosphere from the Hanle effect and surface dynamo simulations. Astrophys J Lett 731(1):L21. https://doi.org/10.1088/2041-8205/731/1/L21. arXiv:1103.5652 [astro-ph.SR]
Shchukina N, Trujillo Bueno J (2015) The impact of surface dynamo magnetic fields on the solar iron abundance. Astron Astrophys 579:A112. https://doi.org/10.1051/0004-6361/201425569
She ZS, Jackson E (1993) On the universal form of energy spectra in fully developed tur bulence. Phys Fluids A 5(7):1526–1528. https://doi.org/10.1063/1.858591
Shporer A, Brown T (2011) The impact of the convective blueshift effect on spectroscopic planetary transits. Astrophys J 733(1):30. https://doi.org/10.1088/0004-637X/733/1/30. arXiv:1103.0775 [astro-ph.EP]
Skoutnev V, Squire J, Bhattacharjee A (2021) Small-scale dynamo in stably stratified turbulence. Astrophys J 906(1):61. https://doi.org/10.3847/1538-4357/abc8ee. arXiv:2008.01025 [physics.flu-dyn]
Smagorinsky J (1963) General circulation experiments with the primitive equations. Mon Weather Rev 91:99. https://doi.org/10.1175/1520-0493(1963)091<0099:GCEWTP>2.3.CO;2
Smitha HN, Anusha LS, Solanki SK et al (2017) Estimation of the magnetic flux emergence rate in the quiet Sun from sunrise data. Astrophys J Suppl Ser 229:17. https://doi.org/10.3847/1538-4365/229/1/17. arXiv:1611.06432 [astro-ph.SR]
Spruit HC (1999) Differential rotation and magnetic fields in stellar interiors. Astron Astrophys 349:189–202. arXiv:astro-ph/9907138 [astro-ph]
Stein RF, Nordlund Å (1998) Simulations of solar granulation. I. General properties. Astrophys J 499:914–933. https://doi.org/10.1086/305678
Stein RF, Nordlund Å (2006) Solar small-scale magnetoconvection. Astrophys J 642(2):1246–1255. https://doi.org/10.1086/501445
Stein RF, Bercik D, Nordlund Å (2003) Solar surface magneto-convection. In: Pevtsov AA, Uitenbroek H (eds) Current theoretical models and future high resolution solar observations: preparing for ATST, p 121. arXiv:astro-ph/0209470
Steiner O, Rezaei R, Schaffenberger W et al (2008) The horizontal internetwork magnetic field: numerical simulations in comparison to observations with Hinode. Astrophys J Lett 680(1):L85. https://doi.org/10.1086/589740. arXiv:0801.4915 [astro-ph]
Steiner O, Salhab R, Freytag B et al (2014) Properties of small-scale magnetism of stellar atmospheres. Publ Astron Soc Jpn 66:S5. https://doi.org/10.1093/pasj/psu083
Subramanian K (1998) Can the turbulent galactic dynamo generate large-scale magnetic fields? Mon Not R Astron Soc 294:718–728. https://doi.org/10.1046/j.1365-8711.1998.01284.x arXiv:astro-ph/9707280 [astro-ph]
Tilgner A, Brandenburg A (2008) A growing dynamo from a saturated Roberts flow dynamo. Mon Not R Astron Soc 391(3):1477–1481. https://doi.org/10.1111/j.1365-2966.2008.14006.x. arXiv:0808.2141 [astro-ph]
Trelles Arjona JC, Martínez González MJ Ruiz Cobo B (2021) Mapping the hidden magnetic field of the quiet Sun. Astrophys J Lett 915(1):L20. https://doi.org/10.3847/2041-8213/ac0af2. arXiv:2106.10546 [astro-ph.SR]
Trujillo Bueno J, del Pino Alemán T (2022) Magnetic field diagnostics in the solar upper atmosphere. Annu Rev Astron Astrophys 60:415–453. https://doi.org/10.1146/annurev-astro-041122-031043
Trujillo Bueno J, Shchukina N, Asensio Ramos A (2004) A substantial amount of hidden magnetic energy in the quiet sun. Nature 430:326–329. https://doi.org/10.1038/nature02669. arXiv:astro-ph/0409004
Vincenzi D (2001) The Kraichnan-Kazantsev dynamo. arXiv e-prints physics/0106090. arXiv:physics/0106090 [physics.flu-dyn]
Vitense E (1953) Die Wasserstoffkonvektionszone der Sonne. Z Astrophys 32:135
Vögler A, Schüssler M (2007) A solar surface dynamo. Astron Astrophys 465:L43–L46. https://doi.org/10.1051/0004-6361:20077253. arXiv:astro-ph/0702681

Wang J, Wang H, Tang F et al (1995) Flux distribution of solar intranetwork magnetic fields. Sol Phys 160:277–288. https://doi.org/10.1007/BF00732808

Warnecke J, Korpi-Lagg M, Gent F et al (2023) Numerical evidence for a small-scale dynamo approaching solar magnetic Prandtl numbers. Nat Astron (accepted). https://doi.org/10.21203/rs.3.rs-1819381/v1

Withbroe GL, Noyes RW (1977) Mass and energy flow in the solar chromosphere and corona. Annu Rev Astron Astrophys 15:363–387. https://doi.org/10.1146/annurev.aa.15.090177.002051

Wright E, Przybylski D, Rempel M et al (2021) Refactoring the MPS/University of Chicago Radiative MHD (MURaM) model for GPU/CPU performance portability using OpenACC directives. In: Proceedings of the platform for advanced scientific computing conference, PASC '21. Association for Computing Machinery, New York. https://doi.org/10.1145/3468267.3470576

Yelles Chaouche L, Moreno-Insertis F, Martínez Pillet V et al (2011) Mesogranulation and the solar surface magnetic field distribution. Astrophys J Lett 727(2):L30. https://doi.org/10.1088/2041-8205/727/2/L30. arXiv:1012.4481 [astro-ph.SR]

Yeo KL, Solanki SK, Krivova NA et al (2020) The dimmest state of the Sun. Geophys Res Lett 47(19):e90243. https://doi.org/10.1029/2020GL090243. arXiv:2102.09487 [astro-ph.SR]

Authors and Affiliations

Matthias Rempel[1] · Tanayveer Bhatia[2] · Luis Bellot Rubio[3] · Maarit J. Korpi-Lagg[2,4,5]

✉ M.J. Korpi-Lagg
maarit.korpi-lagg@aalto.fi

M. Rempel
rempel@ucar.edu

T. Bhatia
bhatia@mps.mpg.de

L. Bellot Rubio
lbellot@iaa.es

1 High Altitude Observatory, National Center for Atmospheric Research, P.O. Box 3000, Boulder, 80307, CO, USA

2 Department of Sun and Heliosphere, Max Planck Institute for Solar System Research, Justus-von-Liebig-Weg 3, Göttingen, 37077, Germany

3 Instituto de Astrofísica de Andalucía, CSIC, Glorieta de la Astronomía s/n, Granada, 18008, Spain

4 Department of Computer Science, Aalto University, Konemiehentie 2, Espoo, 00076, Finland

5 Nordic Institute for Theoretical Physics, KTH Royal Institute of Technology and Stockholm University, Hannes Alvéns väg 12, Stockholm, 10691, Sweden